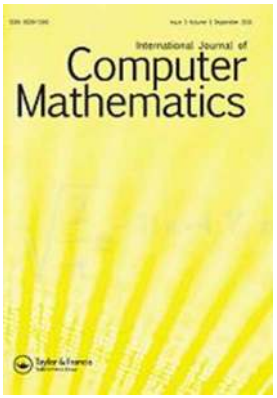

High-order Mixed Weighted Compact and Non-Compact Scheme for Shock and Small Length Scale Interaction

Journal:	*International Journal of Computer Mathematics*
Manuscript ID:	GCOM-2012-0484-B.R1
Manuscript Type:	Original Article
Date Submitted by the Author:	n/a
Complete List of Authors:	Stipcich, Goran; University or Texas at Arlington, Math Fu, Huankun; University or Texas at Arlington, Math Liu, Chaoqun; UT-Arlington, Math
Keywords:	Compact Scheme, WENO, Shock Detector, High Order, High Resolution

High-order Mixed Weighted Compact and Non-Compact Scheme for Shock and Small Length Scale Interaction

G. Stipcich[a], H. Fu[b] and C. Liu[b,*]

[a]*BCAM – Basque Center for Applied Mathematics, Mazarredo14, E48009 Bilbao, Basque Country – Spain;* [b]*University of Texas at Arlington, Arlington, Texas, 76019, USA*

It is critical for a numerical scheme to obtain numerical results as accurate as possible with limited computational resources. Turbulent processes are very sensitive to numerical dissipation, which may dissipate the small length scales. On the other hand, dealing with shock waves, capturing and reproducing of the discontinuity may lead to non-physical oscillations for non-dissipative high-order schemes. In the present work, a new high-order mixed weighted compact and non-compact difference scheme (MWCS hereafter) is proposed for accurate approximation of the derivatives in the governing Euler equations. The basic idea is to recover the non-dissipative high-order weighted compact scheme (WCS) in smooth regions, while linearly combine WCS with a non-compact scheme, the weighted essentially non oscillatory scheme (WENO), for near-shock areas, by using of a shock-detecting function. The proposed formulation does not involve any case-dependent adjustable parameter. A detailed Fourier and local truncation error analysis are used for assessing the dispersion and dissipation characteristics of the scheme. Numerical tests are performed for the one- and two- dimensional case and results are compared with the well established WENO scheme and WCS.

Nomenclature

a,b	=	start, and end point of the one-dimensional domain
C	=	constant optimal weight
c	=	speed of sound
E	=	candidate stencil
E_t	=	total energy per unit volume
F, F_x, F'	=	generic flux function, and its spatial derivatives
$\hat{F}$	=	numerical flux associated with F
H, H'	=	primitive function of $\hat{F}$, and its spatial derivative
h	=	cell size
IS	=	non-linear smoothness indicator
$\mathbf{i}$	=	imaginary unit
i, j, k	=	running indexes
$\hat{k}$	=	wavenumber in the phase space
$\mathbf{i}\hat{k}_e$	=	effective wavenumber in the phase space
N	=	total number of grid points
p	=	pressure

* Corresponding author. Email: cliu@exchange.uta.edu

q, q_t = generic function and its time derivative
t = time
u, v = velocity components along Cartesian coordinate directions
x, y = Cartesian spatial coordinates
α = non-dimensional value of the mixing function
λ = non-dimensional value of the shock-sensor
ρ = density
ω = non-linear weight

I. Introduction

IT is desirable for a numerical scheme to attain high-order accuracy with limited computational resources. In the past two decades, many efforts have been made in developing such high-order schemes, examples being the compact difference schemes[1-3], essentially non-oscillatory[4-6] (ENO) schemes and their weighted variant[7-9] (WENO), discontinuous Gelerkin[10-13] (DG) methods, spectral element[14] (SE) methods, spectral volume methods[15-16] (SVM), spectral difference methods[17-18] (SDM), low dissipative high-order schemes[19], group velocity control schemes[20], and hybrid schemes[21-22].

Physical processes usually have various different length scales. In the case of flow transition and turbulence, for example, small length scales are of great interest and very sensitive to any artificial numerical dissipation. A high order central compact scheme[1,2] (Lele, 1992; Visbal, et al., 2002) is non-dissipative with high-order and high-resolution, and thus appropriate for the solution of flow transition and turbulence cases. However, in many engineering applications such as shock-boundary layer interaction, shock-acoustic interaction, image process, flow in porous media, multiphase flow and detonation wave, there is a presence of both different length scales and shocks/discontinuities.

The shock can be considered as a discontinuity or a mathematical singularity (there is no classical unique solution and the derivatives are not bounded). In the near-shock region, continuity and differentiability of the governing Euler equations are lost and only the weak solution can be obtained. In fluid dynamics it is possible to have a shock solution when considering, for instance, the super-sonic regime of the Euler equations, which are hyperbolic. Hyperbolic systems can be solved taking advantage of the characteristic lines and Riemann invariants. The physics of the shock indicate that the derivative across the shock is not finite, and that the downstream region cannot influence the upstream one. In the framework of finite differences it makes no sense to use, for instance, a high order compact scheme, which takes all grid points on both sides of a shock into account for the numerical approximation of the derivatives. Apparently, the upwind strategies are more suitable than compact schemes in dealing with shocks, and indeed history has shown a great success of upwind technologies applied to hyperbolic systems. Among upwind or bias upwind schemes that are capable to capture a shock sharply, there are Godunov[23], Roe[24], MUSCL[25], TVD[26], ENO[4-6] and WENO[7-8]. All mentioned schemes above are based on upwind or bias upwind technology and are well suited for hyperbolic systems. On the other hand, upwinding strategies are not desirable for solving Navier-Stokes systems, which present a parabolic behavior, and are very sensitive to any numerical dissipation especially when tackling the problem of transitional and turbulent flow, where small length scales are important.

Efforts have been made in developing high-order numerical schemes with high resolution for small length scales, but at the same time capable of sharply capturing the shock/discontinuity without generating visible numerical oscillations. A combination of WENO and standard central scheme is proposed in Ref. 27,28, and a combination of WENO and upwinding compact scheme (UCS) is proposed by Ref. 29, but the mixing function is still complex and has a number of case related adjustable coefficients, which is not convenient to use.

A weighted compact scheme (WCS) is developed by Ref. 30. WCS is based on WENO[7] weighting method for evaluating candidates, which use the standard compact scheme. The building block for each candidate is a Lagrange polynomial in WENO, but is Hermite in WCS, obtaining for the latter a higher order of accuracy with the same stencil width. In shock regions, the WCS controls the contributions of different candidate stencils to minimize the influence of candidates containing a shock/discontinuity. On the other hand, in regions with smooth solution, WCS recovers the standard compact scheme[1] to achieve high accuracy and resolution. Numerical tests reveal that the original WCS works well in some cases such as Burgers' equation, but is not suitable for solving the Euler equations. As mentioned, the usage of derivatives by compact schemes results in global dependency. WCS minimizes the influence of a shock-containing candidate stencil by assigning a smaller weight, but still uses all of the candidates, resulting in global dependency.

In order to overcome the drawback of the WCS, local dependency has to be achieved in shock areas, while recovering global dependency in smooth regions. This fundamental idea leads naturally to the combination of compact and non-compact schemes, that is, to the mixed weighted compact and non-compact scheme (MWCS). The proposed scheme is a linear combination of WCS and WENO schemes, with the aim of taking advantage of the high-resolution property of the WCS in smooth solution regions, and, in near shock regions, employing the WENO scheme, which is non-compact and dissipative. The mixing makes use of a shock-detecting function.

The aim of this work is to develop a high order scheme for those cases where both discontinuities (e.g. shocks) and small length scales (e.g. sound wave, turbulence) are important. The proposed scheme captures the discontinuity (shocks) sharply by upwinding dominant weights, and makes use of the high order compact scheme for high accuracy and high resolution in the smooth area. A black-box type subroutine is developed, which can be used for any discrete data set to achieve high order accuracy for derivatives.

The present work is organized as follows. In Section II the MWCS formulation is described, in Section III contains the Fourier analysis of the scheme, Section IV reports the results of the local truncation error analysis, Section V reports numerical results of test cases for the solution of the Euler equation in the one- and two-dimensional case, including some considerations regarding the computational efficiency, and Section VI concludes the work.

II. Numerical Formulation

The MWCS is a linear combination of the WENO[7,8,31] scheme and WCS[30], where the mixing function relies on a shock-detecting formula. In the present section a description of the three high order schemes along with the mixing function is provided.

To review the different schemes starting from a common framework, it is convenient to consider the scalar conservation equation in the one-dimensional case

$$q_t(x,t) + F_x(q(x,t)) = 0 \tag{2.1}$$

Discretizing the domain, we define a grid (cell interfaces) as

$$a = x_{1/2} < x_{3/2} < \ldots < x_{N-1/2} < x_{N+1/2} = b \tag{2.2}$$

The cell centers and cell sizes are defined, respectively, as

$$x_j \equiv \frac{1}{2}\left(x_{j-1/2} + x_{j+1/2}\right), \quad h_j \equiv x_{j+1/2} - x_{j-1/2}, \quad j = 1,2,\ldots,N$$

The above described grid is shown in Fig. 1, where the dots denote cell centers, and vertical segments denote the cell interfaces (2.2). The candidate stencils of the below revised WENO and WCS schemes are sketched.

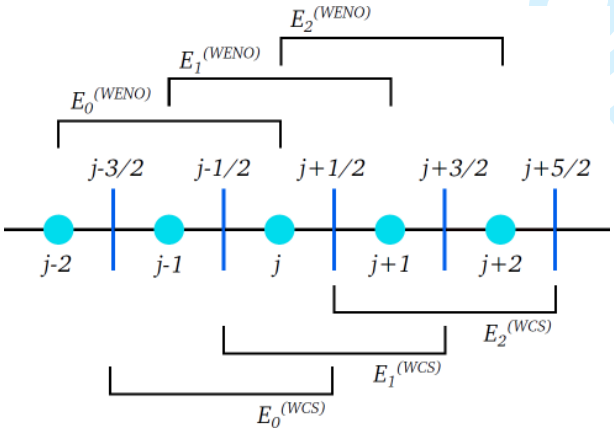

Figure 1. Sketch of the computational grid. The candidate stencils for WENO and WCS schemes are reported.

A semi-discrete conservative form of (2.1) reads as

$$\frac{\mathrm{d}\, q_j}{\mathrm{d}\, t} = -\frac{1}{h_j}\left(\hat{F}_{j+1/2} - \hat{F}_{j-1/2}\right) \tag{2.3}$$

where $\hat{F}$ is the numerical flux associated to the original function F, defined *implicitly* by $F_j = F(q(x_j,t)) \equiv \int_{x_{j-1/2}}^{x_{j+1/2}} \hat{F}(\xi)\mathrm{d}\xi$. With the given implicit definition of the numerical flux $\hat{F}$, Eq. (2.3) constitutes as an *exact* expression of the spatial derivative in Eq. (2.1).

We denote H the primitive function of $\hat{F}(\xi)$, which can be calculated by

$$H_{j+1/2} = H(x_{j+1/2}) = \int_{-\infty}^{x_{j+1/2}} \hat{F}(\xi)\mathrm{d}\xi = \sum_{i=-\infty}^{j} \int_{x_{i-1/2}}^{x_{i+1/2}} \hat{F}(\xi)\mathrm{d}\xi = \sum_{i=-\infty}^{j} F_i\, h_i \tag{2.4}$$

So the primitive function H is calculated from the discrete data set of the original function F. The derivative of the primitive function at the cell interfaces coincides with the numerical flux, i.e.

$$H'_{j+1/2} = \hat{F}_{j+1/2}$$

From the above definitions, it is clear that

$$F_x(x_j) = F'_j = \frac{\hat{F}_{j+1/2} - \hat{F}_{j-1/2}}{h_j} = \frac{H'_{j+1/2} - H'_{j-1/2}}{h_j} \tag{2.5}$$

In the described procedure $F \to H \to \hat{F} \to F'$, introduced by Ref. 4, the only approximation involved is the calculation of the derivative of the primitive function H', whereas all other calculations are exact. The intermediate step through the primitive function H is of crucial importance for the WENO and WCS schemes reviewed in the next paragraphs.

A. The 5th Order Weighted Essentially Non-Oscillatory (WENO) Scheme

The basic idea of the WENO scheme is to obtain a high-order approximation to the numerical flux by a weighted average (convex combination) of multiple lower-order candidate approximations, according to the "smoothness" of the original function on each of the candidates. For obtaining a 5th order WENO scheme, three second-order approximations of the numerical fluxes at $\hat{F}_{j-1/2}$ and $\hat{F}_{j+1/2}$ are obtained from the three candidate stencils (Fig. 1):

$$E_0 = \{F_{j-2}, F_{j-1}, F_j\} \qquad E_1 = \{F_{j-1}, F_j, F_{j+1}\} \qquad E_2 = \{F_j, F_{j+1}, F_{j+2}\}$$

Choosing the Lagrange polynomial for the second order approximation of $\hat{F}_{j+1/2}$, we obtain, for the first stencil:

$$E_0: \quad \hat{F}^{(E_0)}_{j+1/2} \approx \frac{1}{3}F_{j-2} - \frac{7}{6}F_{j-1} + \frac{11}{6}F_j$$

And similarly for the other two stencils E_1 and E_2:

$$E_1: \quad \hat{F}^{(E_1)}_{j+1/2} \approx -\frac{1}{6}F_{j-1} + \frac{5}{6}F_j + \frac{1}{3}F_{j+1} \qquad E_2: \quad \hat{F}^{(E_2)}_{j+1/2} \approx \frac{1}{3}F_j + \frac{5}{6}F_{j+1} - \frac{1}{6}F_{j+2}$$

If we take the weighted average of the three low-order approximations above, with the *constant* optimal weights[7]

$$C_0 = \frac{1}{10} \qquad C_1 = \frac{6}{10} \qquad C_2 = \frac{3}{10} \tag{2.6}$$

we obtain

$$\hat{F}_{j+1/2} \approx \sum_{i=0}^{2} C_i \hat{F}_{j+1/2}^{(E_i)} = \frac{1}{30} F_{j-2} - \frac{13}{60} F_{j-1} + \frac{47}{60} F_j + \frac{9}{20} F_{j+1} - \frac{1}{20} F_{j+2}$$

Note that the constant weights in (2.6) sum up to 1 for consistency, i.e. $\sum_{i=0}^{2} C_i = 1$. After the expression of the approximation for $\hat{F}_{j-1/2} = \hat{F}_{(j-1)+1/2}$ is obtained in analogous fashion as above, we can calculate the discrete approximation to the derivative of the original function F as (see Eq. (2.3))

$$F'_j = \frac{\hat{F}_{j+1/2} - \hat{F}_{j-1/2}}{h_j} \approx \frac{-\frac{1}{30} F_{j-3} + \frac{1}{4} F_{j-2} - F_{j-1} + \frac{1}{3} F_j + \frac{1}{2} F_{j+1} - \frac{1}{20} F_{j+2}}{h_j} \tag{2.7}$$

It is easy to verify by a Taylor series expansion that Eq. (2.7) is a 5th order approximation to the discrete derivative F'_j (see Ref. 32).

Instead of using the constant weights (2.6), the WENO scheme adaptively selects the weights in relation to the "smoothness" of the stencils. The non-linear weights $\omega_{i,j\pm1/2}$ are introduced as[8]

$$\omega_{i,j\pm1/2} = \frac{\gamma_{i,j\pm1/2}}{\sum_{k=0}^{2} \gamma_{k,j\pm1/2}} \qquad \gamma_{i,j\pm1/2} = \frac{C_i}{(\varepsilon + IS_{i,j\pm1/2})^p} \qquad i = 0,1,2 \tag{2.8}$$

where ε is a small parameter which prevents the division by zero, and C_i are those given in (2.6). The parameter p is an important positive integer value which is set equal to 2 in Ref. 8, where the authors found the latter value adequate for obtaining essentially non-oscillatory approximations in applications with shocks. In the present work the same choice $p = 2$ is made for the WENO scheme in all the numerical tests. The indicators $IS_{i,j\pm1/2}$ are associated to the local "smoothness" of the original function F in the i-th stencil E_i (see Ref. 8), and are calculated using the discrete values of the original function. The explicit calculations, for the j+1/2 values (analogue expressions are used for the j-1/2 values), are reported below for reference:

$$E_0: \qquad IS_{0,j+1/2} = \frac{13}{12}\left(F_{j-2} - 2F_{j-1} + F_j\right)^2 + \frac{1}{4}\left(F_{j-2} - 4F_{j-1} + 3F_j\right)^2 \tag{2.9a}$$

$$E_1: \qquad IS_{1,j+1/2} = \frac{13}{12}\left(F_{j-1} - 2F_j + F_{j+1}\right)^2 + \frac{1}{4}\left(F_{j-1} - F_{j+1}\right)^2 \tag{2.9b}$$

$$E_2: \qquad IS_{2,j+1/2} = \frac{13}{12}\left(F_j - 2F_{j+1} + F_{j+2}\right)^2 + \frac{1}{4}\left(F_{j+2} - 4F_{j+1} + 3F_j\right)^2 \tag{2.9c}$$

In general $IS_{k,j-1/2} \neq IS_{k,j+1/2}$, implying that also $\omega_{i,j-1/2} \neq \omega_{i,j+1/2}$. Note that the non-linear weights need to satisfy $\sum_{k=0}^{2} \omega_{k,j\pm1/2} = 1$ for consistency of the scheme. Using the non-linear weights (2.8) for the combination if the candidates, the final form of the WENO scheme reads as

$$\begin{aligned} F'_j = \frac{\hat{F}_{j+1/2} - \hat{F}_{j-1/2}}{h_j} \approx \Bigg[& -\frac{1}{3}\omega_{0,j-1/2} F_{j-3} + \left(\frac{7}{6}\omega_{0,j-1/2} + \frac{1}{3}\omega_{0,j+1/2} + \frac{1}{6}\omega_{1,j-1/2}\right) F_{j-2} + \\ & \left(-\frac{11}{6}\omega_{0,j-1/2} - \frac{7}{6}\omega_{0,j+1/2} - \frac{5}{6}\omega_{1,j-1/2} - \frac{1}{6}\omega_{1,j+1/2} - \frac{1}{3}\omega_{2,j-1/2}\right) F_{j-1} + \\ & \left(\frac{11}{6}\omega_{0,j+1/2} - \frac{1}{3}\omega_{1,j-1/2} + \frac{5}{6}\omega_{1,j+1/2} - \frac{5}{6}\omega_{2,j-1/2} + \frac{1}{3}\omega_{2,j+1/2}\right) F_j + \\ & \left(\frac{1}{3}\omega_{1,j+1/2} + \frac{1}{6}\omega_{2,j-1/2} \frac{5}{6}\omega_{2,j+1/2}\right) F_{j+1} - \frac{1}{6}\omega_{2,j+1/2} F_{j+2} \Bigg] \frac{1}{h_j} \end{aligned} \tag{2.10}$$

From a computational point of view, the WENO scheme produces a *diagonal* matrix of size *N+1*, where the *j*-th row contains the $j-1/2$ -th numerical flux $\hat{F}_{j-1/2}$. The final value of the derivative F'_j is then obtained by Eq. (2.5).

The WENO scheme (2.10) is regarded as a *non-compact* scheme, i.e. the discrete derivative F_j has *local* dependency on the values of the original function F, but not on the derivative at a different point, unlike the WCS described in the next paragraph.

B. The Weighted Compact Scheme (WCS)

The basic idea of WCS[30] is to take a weighted average (convex combination) of two third-order and one fourth-order approximation of the numerical flux $\hat{F}_{j+1/2} = H'_{j+1/2}$, each approximation involving the primitive function H and its derivative H'. Similarly to the WENO scheme, three candidate stencils are defined as

$$E_0 = \{H_{j-3/2}, H_{j-1/2}, H_{j+1/2}\} \qquad E_1 = \{H_{j-1/2}, H_{j+1/2}, H_{j+3/2}\} \qquad E_2 = \{H_{j+1/2}, H_{j+3/2}, H_{j+5/2}\}$$

The approximations for the numerical flux $H'_{j+1/2} = \hat{F}_{j+1/2}$ are obtained making use of compact schemes[1] for the three stencils E_0, E_1, and E_2, respectively, as

$$E_0: \qquad 2H'_{j-1/2} + H'_{j+1/2} \approx \left(-\frac{1}{2}H_{j-3/2} - 2H_{j-1/2} + \frac{5}{2}H_{j+1/2}\right)\frac{1}{h_j} \tag{2.11a}$$

$$E_1: \qquad \frac{1}{4}H'_{j-1/2} + H'_{j+1/2} + \frac{1}{4}H'_{j+3/2} \approx \frac{3(H_{j+3/2} - H_{j-1/2})}{4h_j} \tag{2.11b}$$

$$E_2: \qquad H'_{j+1/2} + 2H'_{j+3/2} \approx \left(-\frac{5}{2}H_{j+1/2} + 2H_{j+3/2} + \frac{1}{2}H_{j+5/2}\right)\frac{1}{h_j} \tag{2.11c}$$

By a Taylor expansion of Eq. (2.11), it can be verified that the candidates E_0 and E_2 give a third-order approximation of $H'_{j+1/2}$, while the candidate E_1 is of fourth-order accuracy[32].

As for WENO, a choice of "optimal" constant weights can be made in order to obtain the highest possible accuracy from the convex combination of the three lower order approximations (2.11). In fact, if the weights are set to the following constant values

$$C_0 = \frac{1}{18} \qquad C_1 = \frac{8}{9} \qquad C_2 = \frac{1}{18} \tag{2.12}$$

the weighted average of the three candidate approximations (2.11) gives the following approximation for $H'_{j+1/2}$

$$\frac{1}{3}H'_{j-1/2} + H'_{j+1/2} + \frac{1}{3}H'_{j+3/2} \approx \left(-\frac{1}{36}H_{j-3/2} - \frac{7}{9}H_{j-1/2} + \frac{7}{9}H_{j+3/2} + \frac{1}{36}H_{j+5/2}\right)\frac{1}{h_j} \tag{2.13}$$

By an analogous procedure, the expression for $H'_{j-1/2} = \hat{F}_{j-1/2}$ is obtained, and making use of Eq. (2.4-2.5) it can be easily shown[32] that Eq. (2.13) recovers exactly the standard sixth order accuracy finite difference compact scheme[1] for the unknown discrete derivative F'_j.

Instead of the constant weights (2.12), we use the non-linear weights (2.8), where the C_i are now those given by (2.12). From the numerical experiments in the one- and two-dimensional cases, we observed that setting $p=1$ in (2.8) for the WCS is an adequate choice in terms of stability and shock-capturing property of the scheme. In the present work we use $p=1$ for the WCS in all the numerical tests. We apply (2.5) to obtain the expression for the final form of the WCS scheme, which reads as

$$\begin{aligned}
&-\left[+3\left(\omega_{0,j-1/2}-\omega_{0,j+1/2}\right)+\frac{3}{2}\left(\omega_{1,j-1/2}-\omega_{1,j+1/2}\right)+3\left(\omega_{2,j-1/2}-\omega_{2,j+1/2}\right)\right]\frac{H'_{j+1/2}}{h_j}+\\
&\left(2\omega_{0,j-1/2}+\frac{1}{4}\omega_{1,j-1/2}\right)F'_{j-1}+\left(3\omega_{0,j-1/2}+\frac{5}{4}\omega_{1,j-1/2}+\omega_{2,j-1/2}-2\omega_{0,j+1/2}-\frac{1}{4}\omega_{1,j+1/2}\right)F'_{j}+\\
&\left(\frac{1}{4}\omega_{1,j+1/2}+2\omega_{2,j+1/2}\right)F'_{j+1}\approx\\
&\left[-\frac{1}{2}\omega_{0,j-1/2}F_{j-2}+\left(-\frac{5}{2}\omega_{0,j-1/2}-\frac{3}{4}\omega_{1,j-1/2}+\frac{1}{2}\omega_{0,j+1/2}\right)F_{j-1}+\right.\\
&\left(-\frac{3}{4}\omega_{1,j-1/2}-\frac{5}{2}\omega_{2,j-1/2}+\frac{5}{2}\omega_{0,j+1/2}+\frac{3}{4}\omega_{1,j+1/2}\right)F_{j}+\\
&\left.\left(-\frac{1}{2}\omega_{2,j-1/2}+\frac{3}{4}\omega_{1,j+1/2}+\frac{5}{2}\omega_{2,j+1/2}\right)F_{j+1}+\frac{1}{2}\omega_{2,j+1/2}F_{j+2}\right]\frac{1}{h_j}
\end{aligned} \tag{2.14}$$

For the WCS (2.14), a *tri-diagonal* matrix of size *N+1* has to be solved. The *j*-th row contains the j-1/2-th numerical flux $H'_{j-1/2} = \hat{F}_{j-1/2}$ and the final value of the derivative F'_j is obtained using Eq. (2.5).

The WCS (2.14) involves also the derivatives at different points, F'_{j-1} and F'_{j+1}, thus resulting in a *compact* scheme, i.e. the WCS has *global* dependency.

C. The Mixed Weighted Compact and Non-Compact Scheme (MWCS)

The MWCS linearly combines the two schemes described in the previous paragraphs, WENO and WCS. As it is described in detail in Section III using the Fourier analysis and in Section IV considering the local truncation errors, comparing the WENO and WCS schemes the first one has lower resolution and it has a certain amount of dissipative

error, while WCS has higher resolution and no dissipation in smooth areas. Numerical results presented in Section V confirm that:

- WENO scheme is capable of capturing the shock without generating unphysical oscillations, but excessively smears the shock and small length scales.

- WCS is more accurate and captures the shock more sharply, but unfortunately, due to the absence of dissipation in smooth areas, the scheme allows unphysical oscillations generated by shocks to grow in smooth areas without being dissipated. The WCS thus results to be unstable, especially in multidimensional applications.

The above concepts lead to the idea of a *mixing function* which linearly combines the two schemes in order to ensure numerical stability on one hand, and to obtain a sharp shock-capturing and good resolution for small length scales on the other. The resulting formulation of the MWCS numerical flux reads as

$$\hat{F}_{j-1/2}^{(MWCS)} = \alpha_j \hat{F}_{j-1/2}^{(WCS)} + (1-\alpha_j)\hat{F}_{j-1/2}^{(WENO)} \tag{2.15}$$

and for consistency of the scheme we must satisfy $0 \le \alpha \le 1$. Virtually, with $\alpha = 0$ the WENO scheme is recovered, and with $\alpha = 1$ the WCS is recovered.

D. The Mixing Function

The value of α in Eq. (2.15) is calculated *locally* making use of a shock-detecting formula. Physically, a shock wave is characterized by the sudden *compression* of the flow taking place in a very restricted space, and the values of the velocity, pressure, and density are subject to a discontinuous jump across the shock. Several methods for estimating the location of a shock, or, roughly speaking, the local "smoothness" of the solution, have been proposed, examples being the Harten switch[33] or an improvement of it proposed in Ref. 32. The WENO weights (2.8) proposed by Ref. 8 themselves can be considered a shock-locating function. In the present study, the following shock-sensor, inspired by Ref. 34, is proposed

$$\lambda_i = \frac{1}{2}\left[1 - \tanh\left(2.5 + d_s \frac{h_i}{c_i}\nabla\cdot\mathbf{u}\right)\right] \tag{2.16}$$

where $\mathbf{u}$ is the velocity vector. The term $h/c\,\nabla\cdot\mathbf{u}$ is the dimensionless dilatation, where the term h/c properly nondimensionalizes the numerical dilatation, regardless the particular nondimensionalization used for the rest of the variables in the equations[34]. The factor $h/c\,\nabla\cdot\mathbf{u}$ can be interpreted as a ratio between the time scales of the highest frequency acoustic wave that can be resolved on the grid and the time scale of the compression:

$$\frac{h}{c}\nabla\cdot\mathbf{u} = \frac{\tau_{max.}}{2\tau_{compr.}}$$

(the factor $2h/c$ identifies the time scale of the highest frequency which can be captured by the specific grid[35]). The scaling factor d_s "sharpens" the hyperbolic tangent function and is set to $d_s = 10$ in Ref. 34, while in the present work it is set $d_s = 40$, since the formula is meant to detect both strong and minor shocks. The given sensor (2.16) is activated (i.e. the value of λ raises from 0 to 1 for smooth and shock areas, respectively) only for compressions, i.e. for *negative* values of the divergence of the velocity vector, and only when the magnitudes of the period of the acoustic wave is comparable to the magnitude of the dilatation. In particular, the sensor is activated when the time scale of the period of the acoustic wave $\tau_{max.}$ is comparable to 1/20th of the time scale of the dilatation (shock) $\tau_{compr.}$, since we have:

$$d_s\frac{h}{c}\nabla\cdot\mathbf{u} = \frac{\tau_{max.}}{2\tau_{compr.}} \Rightarrow \tau_{max.} = \frac{2}{d_s}\tau_{compr.} = \frac{1}{20}\tau_{compr.}$$

In order to eliminate cusps in the values of λ, the approximate truncated-Gaussian filter as in Ref. 35 is applied on each grid line sequentially

$$\overline{\lambda}_i = \frac{3565}{10368}\lambda_i + \frac{3091}{12960}(\lambda_{i-1}+\lambda_{i+1}) + \frac{1997}{25920}(\lambda_{i-2}+\lambda_{i+2}) + \frac{149}{12960}(\lambda_{i-3}+\lambda_{i+3})\frac{149}{103680}(\lambda_{i-4}+\lambda_{i+4}) \tag{2.17}$$

where the overbar indicates the filtered quantity. The filtered values at the near-boundary points ($i=1,...,4$ and $i=N-3,...,N$) are obtained by reflection across the boundary. The performance of the given shock-sensor is assessed through the numerical experiments shown in Section V.

In order to attain numerical stability, the WCS needs to be combined with WENO in the whole domain (especially in the multi-dimensional case) as the absence of dissipation for the WCS leads to numerical oscillations generated in the shock areas. Hence, to calculate the final mixing value α in (2.15), the following expression is proposed

$$\alpha_i = 0.75*(1.0-\overline{\lambda}_i) \tag{2.18}$$

Expression (2.18) smoothly varies from 0.0 to 0.75, according to the smoothness of the function as given from the sensor (2.16), thus allowing the scheme to dynamically make use of a mixture of WENO and WCS. The scheme automatically uses up to 75% of WCS in smooth areas ($\overline{\lambda}_i \cong 0$), while turning to WENO in shock areas ($\overline{\lambda}_i \cong 1$).

III. Fourier Analysis

The Fourier analysis[36,37] has been used to quantify the dispersion and dissipation errors of the proposed MWCS. The Fourier analysis provides an effective insight into resolution and diffusion properties of the MWCS, which may be used to further improve the mixing function proposed in Eq. (2.18).

In the present section, the Fourier analysis of the first order derivative is performed for the three schemes. The presence of the WENO weights (2.8) introduce a non-linearity in expressions (2.10) and (2.14), being that the calculation of the "smoothness" indicators $IS_{i,j\pm1/2}$ (2.9) involves the original function F (see Ref. 8), which would lead to the combination of different Fourier coefficients. Therefore, a reasonable simplification is to consider the non-linear weights as constants. Furthermore, the assumption $\omega_{i,j-1/2}=\omega_{i,j+1/2}=\omega_i$, $i=1,2,3$ is made for simplicity.

Following Ref. 36, the modified, or effective, wavenumber $\mathbf{i}\hat{k}_e$ of the WENO scheme (2.10), where $\mathbf{i}$ indicates the imaginary unit number $\mathbf{i}=\sqrt{-1}$, reads as

$$\mathbf{i}\hat{k}_e^{(WENO)} = \frac{11}{6}\omega_0 + \frac{1}{2}\omega_1 - \frac{1}{2}\omega_2 + \left(-3\omega_0 - \frac{2}{3}\omega_1 + \frac{2}{3}\omega_2\right)\sin\hat{k} + \left(\frac{3}{2}\omega_0 + \frac{1}{6}\omega_1 - \frac{1}{6}\omega_2\right)\sin 2\hat{k} - \frac{1}{3}\omega_0\sin 3\hat{k} + \mathbf{i}\left[\left(3\omega_0 + \frac{4}{3}\omega_1 + \frac{4}{3}\omega_2\right)\sin\hat{k} + \left(-\frac{3}{2}\omega_0 - \frac{1}{6}\omega_1 - \frac{1}{6}\omega_2\right)\sin 2\hat{k} + \frac{1}{3}\omega_0\sin 3\hat{k}\right] \tag{3.1}$$

analogously, the modified wavenumber of the WCS (2.14) reads as

$$\mathbf{i}\hat{k}_e^{(WCS)} = \Big[(\omega_0-\omega_2)\big(5-4\cos\hat{k}-\cos 2\hat{k}\big)+ \mathbf{i}\Big((4\omega_0+3\omega_1+4\omega_2)\sin\hat{k}+(\omega_0+\omega_2)\sin 2\hat{k}\Big)\Big] \Big/ \Big[(4\omega_0+\omega_1+4\omega_2)\cos\hat{k}+2(\omega_0+\omega_1+\omega_2)-4\mathbf{i}(\omega_0-\omega_2)\sin\hat{k}\Big] \tag{3.2}$$

where $\hat{k}\in(0,\pi)$ is the wavenumber.

The dispersion error, or rather the resolution of the scheme, is quatified by the imaginary part of the modified wavenumber $\mathrm{Im}(\mathbf{i}\hat{k}_e)$, while the real part $\mathrm{Re}(\mathbf{i}\hat{k}_e)$ is related to dissipation. Dispersion errors are waves, corresponding to different wavenumbers, which travel at different velocity. The imaginary part of the effective wavenumber $\mathrm{Im}(\mathbf{i}\hat{k}_e)$ represents dispersion, i.e. the phase or frequency error in representing the different wavenumbers of the spectrum. Dissipation or diffusion errors, associated to the negative of the real part of the modified wavenumber $-\mathrm{Re}(\mathbf{i}\hat{k}_e)$, constitute the amplification error, either positive or negative, introduced by the numerical scheme.

In the following paragraphs, the dispersion and dissipation characteristics of WENO, WCS and MWCS are assessed for smooth and shock areas. In *smooth* regions, the non-linear weights (2.8) tend to assume their optimal values (2.6) for WENO and (2.12) for WCS, and we substitute the respective optimal weights into expressions (3.1) and (3.2) for the effective wavenumber. In order to test the schemes in shock regions, we substitute the "extreme" values of the weights (i.e. one of the weights is equal to 1 and the other two are null) are substituted into (3.1) and (3.2). In order to obtain the dispersion error for the MWCS, the same linear combination as in (2.15) is applied to the errors of WENO and WCS, and three values of the mixing parameter $\bar{\lambda}=0.0,0.4,0.9$ in (2.18) are considered for reference.

Smooth regions: optimal values of the non-linear weights

We substitute in the expressions for the modified wavenumbers (3.1) and (3.2) for WENO and WCS the respective optimal weights (2.6) and (2.12).

For obtaining the *dispersion* error, the *imaginary* parts of the resulting effective wavenumbers have to be considered

$$\mathrm{Im}(\mathbf{i}\hat{k}_e^{(WENO)}) = \frac{3}{2}\sin\hat{k}-\frac{3}{10}\sin 2\hat{k}+\frac{1}{30}\sin 3\hat{k} \tag{3.3a}$$

$$\mathrm{Im}(\mathbf{i}\hat{k}_e^{(WCS)}) = \frac{\big(14+\cos\hat{k}\big)\sin\hat{k}}{9+6\cos\hat{k}} \tag{3.3b}$$

where, due to the definition of the WCS, it is clear that the expression for the dispersion error of the WCS (3.3b) coincides with the dispersion error calculated for the standard sixth order compact scheme[1]. Figure 2 shows the dispersion errors w.r.t. the wavenumber $\hat{k}$ of the MWCS, WENO and WCS for smooth regions. It can be observed that:

- the resolution of the MWCS is better than WENO scheme for decreasing values of the mixing parameter $\bar{\lambda}$, over the whole range of the wavenumber $\hat{k}$;
- the WCS shows to possess the best resolution especially at higher values of the wavenumber $\hat{k}$.

We obtain the *dissipation* errors by considering the *real* parts of the resulting effective wavenumbers

$$\mathrm{Re}(\mathbf{i}\hat{k}_e^{(WENO)}) = \frac{1}{3}-\frac{1}{2}\cos\hat{k}+\frac{1}{5}\cos 2\hat{k}-\frac{1}{30}\cos 3\hat{k} \tag{3.4a}$$

$$\mathrm{Re}(\mathbf{i}\hat{k}_e^{(WCS)}) = 0 \tag{3.4b}$$

Figure 3 reports the dissipation errors w.r.t. the wavenumber $\hat{k}$ of the MWCS, WENO and WCS for smooth regions. The following considerations can be drawn:

- the WENO scheme is dissipative over the middle and high range of the wavenumber $\hat{k}$;
- the WCS is characterized by the absence of dissipation error being that, for smooth regions, the WCS recovers the standard sixth order compact scheme[1];
- the MWCS is characterized by a certain (low) amount of dissipative error over the middle and high wavenumber range, due to the WENO component which increases with $\overline{\lambda}$.

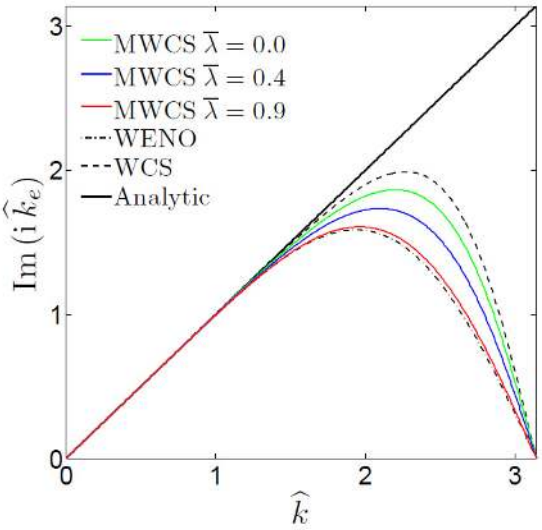

Figure 2. Dispersion error in smooth regions.

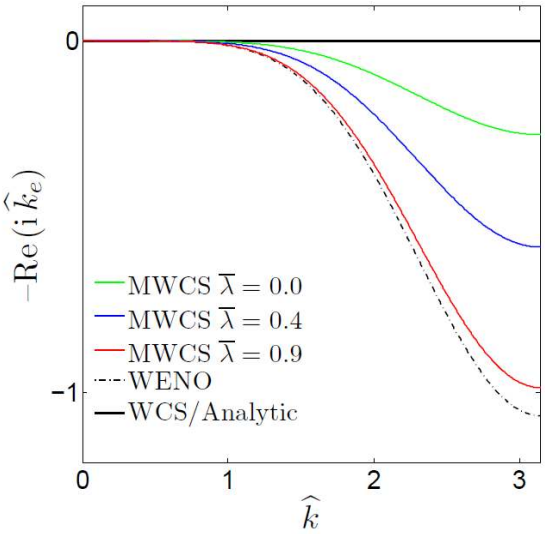

Figure 3. Dissipation error in smooth regions.

Shock region: using only stencil E_0

We assume that the stencils E_1 and E_2 defined in Section II contain a shock, therefore we substitute the following values of the linear weights

$$\omega_0 = 1, \omega_1 = \omega_2 = 0 \tag{3.5}$$

into the expressions of the effective wavenumbers (3.1) and (3.2) for WENO and WCS respectively.

The *dispersion* error corresponds to the *imaginary* part of the resulting effective wavenumbers

$$\mathrm{Im}(\mathbf{i}\hat{k}_e^{(WENO)}) = 3\sin\hat{k} - \frac{3}{2}\sin 2\hat{k} + \frac{1}{3}\sin 3\hat{k} \tag{3.6a}$$

$$\mathrm{Im}(\mathbf{i}\hat{k}_e^{(WCS)}) = \frac{(8+\cos\hat{k})\sin\hat{k}}{5+4\cos\hat{k}} \tag{3.6b}$$

Figure 4 reports the dispersion errors w.r.t. the wavenumber $\hat{k}$ for WENO, WCS and MWCS when only stencil E_0 is used. The following conclusion can be drawn:

- WENO resolution is confined to the low wavenumbers' range;

- the resolution of MWCS is improved w.r.t. WENO over the whole range of wavenumbers as the mixing value $\overline{\lambda}$ decreases.

The *dissipation* error is associated with the *real* part of the resulting effective wavenumbers

$$\mathrm{Re}(\mathbf{i}\hat{k}_e^{(WENO)}) = \frac{11}{6} - 3\cos\hat{k} + \frac{3}{2}\cos 2\hat{k} - \frac{1}{3}\cos 3\hat{k} \tag{3.7a}$$

$$\mathrm{Re}(\mathbf{i}\hat{k}_e^{(WCS)}) = -\frac{4\sin\left(\hat{k}/2\right)^4}{5+4\cos\hat{k}} \tag{3.7b}$$

Figure 5 shows the corresponding dissipation errors of the different numerical schemes, when only stencil E_0 is used. The following considerations can be drawn:

- the WENO scheme is predominantly dissipative over the high wavenumber range;
- the WCS possesses a certain amount of *positive* dissipation error (i.e. amplification error) for high wavenumbers;
- the MWCS is dissipative over the whole wavenumber range, and the error is lower w.r.t. WENO.

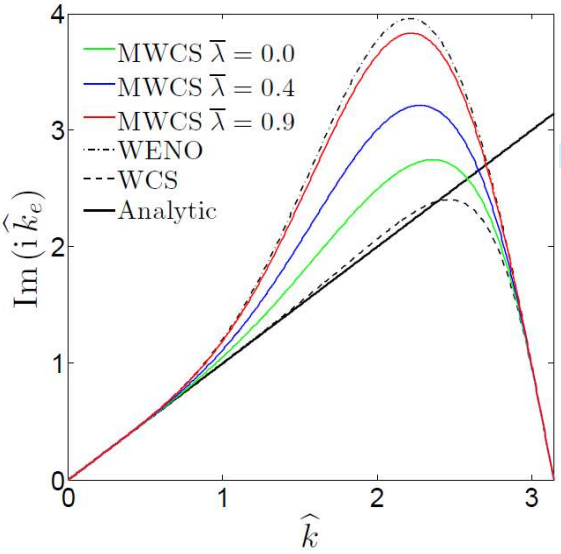

Figure 4. Dispersion error in shock regions: only stencil E_0 is used.

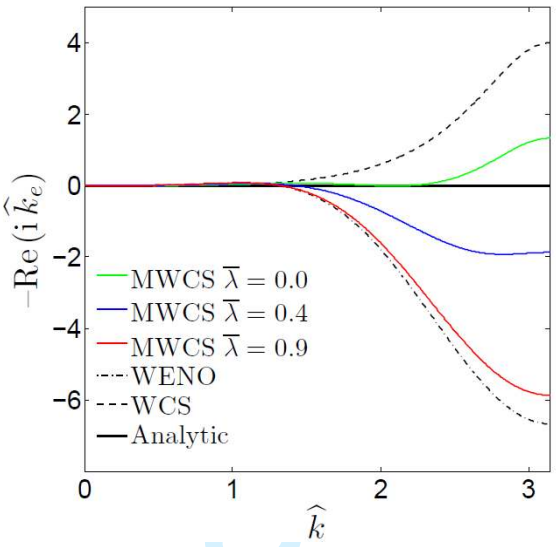

Figure 5. Dissipation error in shock regions: only stencil E_0 is used.

Shock region: using only stencil E_1

In this case, we assume that the stencils E_0 and E_2 contain a shock, therefore we substitute the following values of the linear weights

$$\omega_0 = 0, \omega_1 = 1, \omega_2 = 0 \tag{3.8}$$

into the expressions of the effective wavenumbers (3.1) and (3.2) for WENO and WCS respectively.

The *dispersion* error, associated to the *imaginary* part of the resulting effective wavenumber, reads as

$$\mathrm{Im}(\mathbf{i}\hat{k}_e^{(WENO)}) = \frac{4}{3}\sin\hat{k} - \frac{1}{6}\sin 2\hat{k} \tag{3.9a}$$

$$\mathrm{Im}(\mathbf{i}\hat{k}_e^{(WCS)}) = \frac{3\sin\hat{k}}{2+\cos\hat{k}} \tag{3.9b}$$

where, due to the definition of the WCS, the expression for the dispersion error of the WCS (3.9b) coincides with the dispersion error calculated for the fourth order compact scheme[1]. Figure 6 shows the dispersion error of the different schemes w.r.t. the wavenumber $\hat{k}$, when only the stencil E_1 is used. The following considerations can be drawn:

- the resolution of WENO scheme is confined to the low wavenumber range;
- the resolution of the MWCS is better than WENO over the whole wavenumber range as the mixing value $\overline{\lambda}$ decreases, thus augmenting the WCS component.

The *dissipation* error, quantified as the *real* part of the resulting effective wavenumbers, reads as

$$\mathrm{Re}(\mathbf{i}\hat{k}_e^{(WENO)}) = \frac{1}{2} - \frac{2}{3}\cos\hat{k} + \frac{1}{6}\cos 2\hat{k} \tag{3.10a}$$

$$\mathrm{Re}(\mathbf{i}\hat{k}_e^{(WCS)}) = 0 \tag{3.10b}$$

Figure 7 reports the plot of the dissipation errors for the considered schemes w.r.t. the wavenumber $\hat{k}$, when only the stencil E_1 is used. The following conclusions are drawn:

- the WENO scheme is dissipative over almost the whole wavenumber range, especially at the higher frequencies;
- the WCS is free from dissipation error;
- the MWCS possesses a lower amount of dissipative error w.r.t. WENO, over the whole wavenumber range.

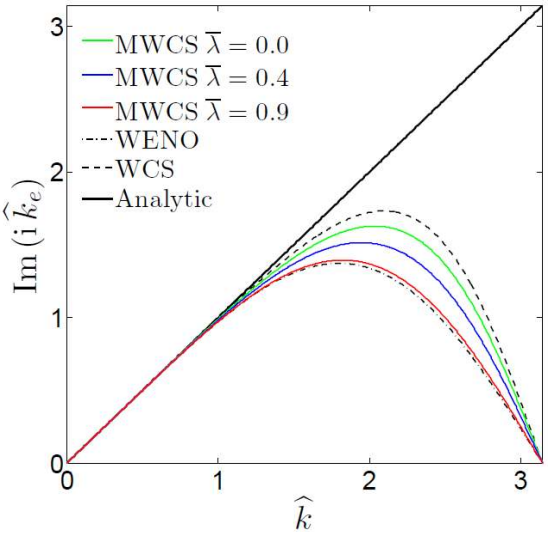

Figure 6. Dispersion error in shock regions: only stencil E_1 is used.

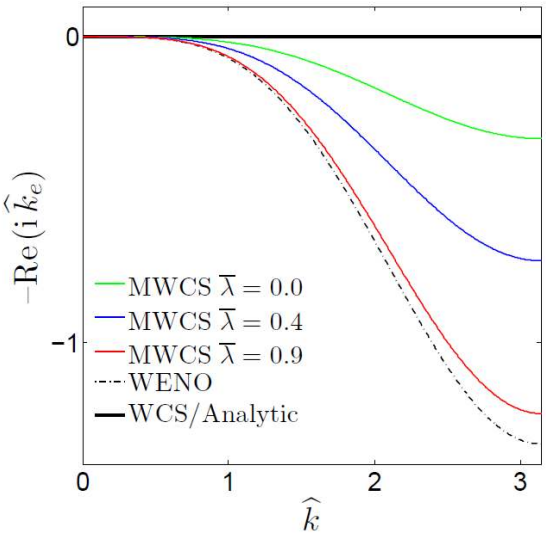

Figure 7. Dissipation error in shock regions: only stencil E_1 is used.

Shock region: using only stencil E_2

In the last case considered, we assume that the stencils E_0 and E_1 contain a shock, therefore we substitute the following values of the linear weights

$$\omega_0 = \omega_1 = 0,\ \omega_2 = 1 \tag{3.11}$$

into the expressions of the effective wavenumbers (3.1) and (3.2) for WENO and WCS respectively.

The *dispersion* error is obtained by considering the *imaginary* part of the resulting modified wavenumber

$$\mathrm{Im}(\mathbf{i}\hat{k}_e^{(WENO)}) = \frac{4}{3}\sin\hat{k} - \frac{1}{6}\sin 2\hat{k} \tag{3.12a}$$

$$\mathrm{Im}(\mathbf{i}\hat{k}_e^{(WCS)}) = \frac{(8+\cos\hat{k})\sin\hat{k}}{5+4\cos\hat{k}} \tag{3.12b}$$

Figure 8 shows the dispersion characteristics of the considered schemes w.r.t. the wavenumber $\hat{k}$, when only the stencil E_2 is used. The following conclusions are drawn:

- the WENO resolution is confined to the low wavenumber range;
- the WCS has good resolution over the low and middle wavenumber range;
- the MWCS has improved resolution, w.r.t. WENO, due to the mixing with WCS as $\overline{\lambda}$ decreases;
- the stencils E_1 and E_2 of WENO scheme have equal resolution errors;
- the stencils E_0 and E_2 of WCS have equal resolution errors.

The dissipation error is obtained by considering the real part of the resulting effective wavenumber

$$\mathrm{Re}(\mathbf{i}\hat{k}_e^{(WENO)}) = -\frac{1}{2} + \frac{2}{3}\cos\hat{k} - \frac{1}{6}\cos 2\hat{k} \tag{3.13a}$$

$$\mathrm{Re}(\mathbf{i}\hat{k}_e^{(WCS)}) = \frac{4\sin\left(\hat{k}/2\right)^4}{5+4\cos\hat{k}} \tag{3.13b}$$

Figure 9 reports the dissipation error of the considered WENO, WCS and WCS, w.r.t. the wavenumber $\hat{k}$, when only the stencil E_2 is used. The following considerations can be drawn:

- the WENO scheme have a certain amount of *positive* dissipation error (i.e. amplification) at middle and high wavenumber range;
- the WCS is dissipative over the middle and high wavenumber range;
- the resulting MWCS has a smaller amount of dissipative error w.r.t. both WENO and WCS over the whole wavenumber range;
- depending on the mixing value $\overline{\lambda}$, the MWCS possesses a certain amount (lower w.r.t. to WENO) of *positive* dissipation error;
- the stencils E_1 and E_2 of WENO scheme have equal dissipation errors in magnitude, but with opposite signs;
- the stencils E_0 and E_2 of WCS have equal dissipation errors in magnitude, but with opposite signs.

The Fourier analysis reveals that when using only stencil E_0 or E_2, the dissipation error is lower than WCS. When using only stencil E_2, the scheme shows some amount of positive dissipation error, which represents an amplification error and can be related to the instability of the method. Nevertheless, this is an extreme situation and the amount of positive dissipation error is lower than that of the pure WENO or WCS. The scheme is overall dissipative and thus stable. The proposed MWCS has better resolution properties w.r.t. WENO scheme in all considered cases, although it does not attain the good resolution characteristics of WCS. The amount of dissipation error of the MWCS is lower w.r.t. WENO for all considered cases, but higher compared to WCS. The (negative)

dissipation associated to MWCS, tough, ensures its stability. Numerical results presented in Section V confirm the results of the Fourier analysis.

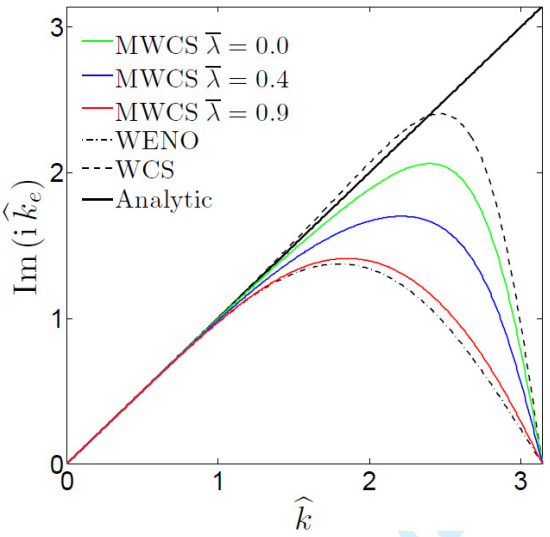

Figure 8. Dispersion error in shock regions: only stencil E_2 is used.

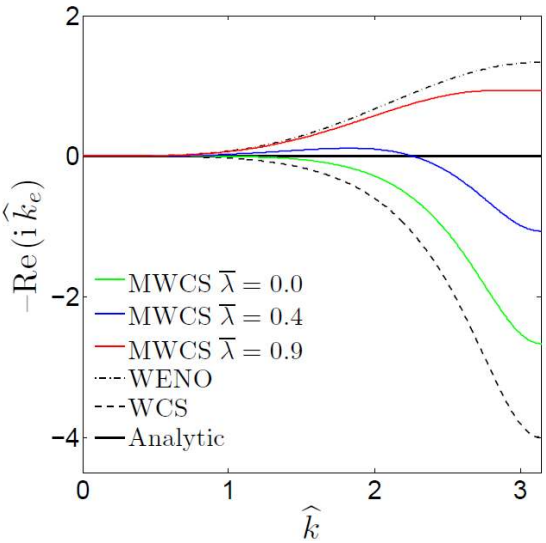

Figure 9. Dissipation error in shock regions: only stencil E_2 is used.

IV. Local Truncation Error Analysis

In addition to the Fourier analysis presented in section III, dissipation and dispersion errors may be assessed in terms of local truncation errors. The truncation error of a numerical scheme is defined as

$$\tau \equiv F'(x_j) - F'_j \tag{4.1}$$

where $F'(x_j)$ is the exact value of the derivative and F'_j is the approximation calculated by the numerical scheme. The the assumption $\omega_{i,j-1/2} = \omega_{i,j+1/2} = \omega_i$, $i = 1,2,3$ is made for simplicity. After a Taylor expansion of Eq. (4.1) at the point x_j is performed, the following truncation errors are obtained for the WENO and WCS schemes, respectively

$$\begin{aligned}\tau^{(WENO)} = {} & \frac{1}{12}(3\omega_0 - \omega_1 + \omega_2)h^3 \frac{\partial^4 F_j}{\partial x^4} + \frac{1}{30}(-9\omega_0 + \omega_1 + \omega_2)h^4 \frac{\partial^5 F_j}{\partial x^5} + \\ & \frac{1}{72}(15\omega_0 - \omega_1 + \omega_2)h^5 \frac{\partial^6 F_j}{\partial x^6} + \frac{1}{252}(-27\omega_0 + \omega_1 + \omega_2)h^6 \frac{\partial^7 F_j}{\partial x^7} + \\ & \frac{1}{960}(43\omega_0 - \omega_1 + \omega_2)h^7 \frac{\partial^8 F_j}{\partial x^8} + \frac{1}{4320}(-69\omega_0 + \omega_1 + \omega_2)h^8 \frac{\partial^9 F_j}{\partial x^9} + \\ & \frac{1815\omega_0 + 17(-\omega_1 + \omega_2)}{362880} h^9 \frac{\partial^{10} F_j}{\partial x^{10}} + \frac{-2779\omega_0 + 17(\omega_1 + \omega_2)}{1995840} h^{10} \frac{\partial^{11} F_j}{\partial x^{11}} + o(h^{12})\end{aligned} \tag{4.2a}$$

$$\tau^{(WCS)} = \frac{1}{12}(\omega_0 - \omega_2)h^3 \frac{\partial^4 F}{\partial x^4} + \frac{1}{120}(-8\omega_0 + \omega_1 - 8\omega_2)h^4 \frac{\partial^5 F}{\partial x^5} + \frac{11}{360}(\omega_0 - \omega_2)h^5 \frac{\partial^6 F}{\partial x^6} + \frac{1}{2520}(-26\omega_0 + \omega_1 - 26\omega_2)h^6 \frac{\partial^7 F}{\partial x^7} + \frac{19}{6720}(\omega_0 - \omega_2)h^7 \frac{\partial^8 F}{\partial x^8} + \frac{1}{120960}(-80\omega_0 + \omega_1 - 80\omega_2)h^8 \frac{\partial^9 F}{\partial x^9} + \frac{257(\omega_0 - \omega_2)}{1814400}h^9 \frac{\partial^{10} F}{\partial x^{10}} - \frac{684\omega_0 + \omega_1 + 684\omega_2}{26611200}h^{10} \frac{\partial^{11} F}{\partial x^{11}} + o(h^{12}) \quad (4.2b)$$

The *even* derivative terms in the above Eq. (4.2) are related to the amplification error, i.e. the *dissipation* error may be quantified simply by taking the even derivative terms in Eq. (4.2), obtaining

$$\tau_{diss}^{(WENO)} = \frac{1}{12}(3\omega_0 - \omega_1 + \omega_2)h^3 \frac{\partial^4 F_j}{\partial x^4} + \frac{1}{72}(15\omega_0 - \omega_1 + \omega_2)h^5 \frac{\partial^6 F_j}{\partial x^6} + \frac{1}{960}(43\omega_0 - \omega_1 + \omega_2)h^7 \frac{\partial^8 F_j}{\partial x^8} + \frac{1815\omega_0 + 17(-\omega_1 + \omega_2)}{362880}h^9 \frac{\partial^{10} F_j}{\partial x^{10}} + o(h^{12}) \quad (4.3a)$$

$$\tau_{diss}^{(WCS)} = \frac{1}{12}(\omega_0 - \omega_2)h^3 \frac{\partial^4 F}{\partial x^4} + \frac{11}{360}(\omega_0 - \omega_2)h^5 \frac{\partial^6 F}{\partial x^6} + \frac{19}{6720}(\omega_0 - \omega_2)h^7 \frac{\partial^8 F}{\partial x^8} + \frac{257(\omega_0 - \omega_2)}{1814400}h^9 \frac{\partial^{10} F}{\partial x^{10}} + o(h^{12}) \quad (4.3b)$$

Analogously, the phase error is related to the *odd* derivative terms, o rather, the *dispersion* errors are determined by the odd derivative terms in Eq. (4.2), obtaining

$$\tau_{disp}^{(WENO)} = \frac{1}{30}(-9\omega_0 + \omega_1 + \omega_2)h^4 \frac{\partial^5 F_j}{\partial x^5} + \frac{1}{252}(-27\omega_0 + \omega_1 + \omega_2)h^6 \frac{\partial^7 F_j}{\partial x^7} + \frac{1}{4320}(-69\omega_0 + \omega_1 + \omega_2)h^8 \frac{\partial^9 F_j}{\partial x^9} + \frac{-2779\omega_0 + 17(\omega_1 + \omega_2)}{1995840}h^{10} \frac{\partial^{11} F_j}{\partial x^{11}} + o(h^{13}) \quad (4.4a)$$

$$\tau_{disp}^{(WCS)} = \frac{1}{120}(-8\omega_0 + \omega_1 - 8\omega_2)h^4 \frac{\partial^5 F}{\partial x^5} + \frac{1}{2520}(-26\omega_0 + \omega_1 - 26\omega_2)h^6 \frac{\partial^7 F}{\partial x^7} + \frac{1}{120960}(-80\omega_0 + \omega_1 - 80\omega_2)h^8 \frac{\partial^9 F}{\partial x^9} - \frac{684\omega_0 + \omega_1 + 684\omega_2}{26611200}h^{10} \frac{\partial^{11} F}{\partial x^{11}} + o(h^{13}) \quad (4.4b)$$

In the following paragraphs, the truncation errors of WENO, WCS and MWCS are analyzed for smooth and shock areas. In *smooth* regions, the non-linear weights (2.8) tend to assume their optimal values (2.6) for WENO and (2.12) for WCS, and we substitute the respective optimal weights into expressions (4.2a) and (4.2b) for the complete form of the truncation error. In order to test the schemes in shock regions, the "extreme" values of the weights (i.e. one of the weights is equal to 1 and the other two are null) are substituted into (4.2). The value of the truncation error for the MWCS is obtained by applying the same linear combination as in (2.15) to the errors of WENO and WCS, and three values of the mixing parameter $\overline{\lambda} = 0.0, 0.4, 0.9$ in (2.18) are considered for reference.

Smooth regions: optimal values of the non-linear weights

The optimal values for the non-linear weights ω of Eq. (2.6) and (2.12) are substituted into Eq. (4.2a) and (4.2b) for WENO and WCS respectively, giving the truncation error for smooth regions

$$\tau^{(WENO)} = \frac{1}{60}h^5\frac{\partial^6 F_j}{\partial x^6} - \frac{1}{140}h^6\frac{\partial^7 F_j}{\partial x^7} + \frac{1}{240}h^7\frac{\partial^8 F_j}{\partial x^8} - \frac{1}{720}h^8\frac{\partial^9 F_j}{\partial x^9} + \frac{7}{14400}h^9\frac{\partial^{10} F_j}{\partial x^{10}} - \frac{7}{52800}h^{10}\frac{\partial^{11} F_j}{\partial x^{11}} + o\left(h^{12}\right) \tag{4.5a}$$

$$\tau^{(WCS)} = -\frac{1}{1260}h^6\frac{\partial^7 F}{\partial x^7} - \frac{1}{15120}h^8\frac{\partial^9 F}{\partial x^9} - \frac{173}{59875200}h^{10}\frac{\partial^{11} F}{\partial x^{11}} + o\left(h^{12}\right) \tag{4.5b}$$

where, as already stated in Section II, it is observed that the WENO and WCS schemes are respectively of 5th and 6th order accuracy in smooth regions. Expression (4.5b) for the truncation error of the WCS scheme is free from even derivative terms, which confirms the results of the Fourier analysis in Section III, i.e. WCS is free from dissipation errors in smooth regions. Figure 10 reports the truncation errors for the three considered schemes WENO, WCS and MWCS, in the form of a bar plot with respect to the different considered orders. The following conclusions can be drawn:

- the MWCS has lower truncation error w.r.t. WENO at any considered order;
- the WCS truncation error is considerably lower w.r.t. WENO for any considered order;
- for the MWCS, the magnitude of the leading error term is $\sim 10^{-3}h^5$, and decreases for higher orders.

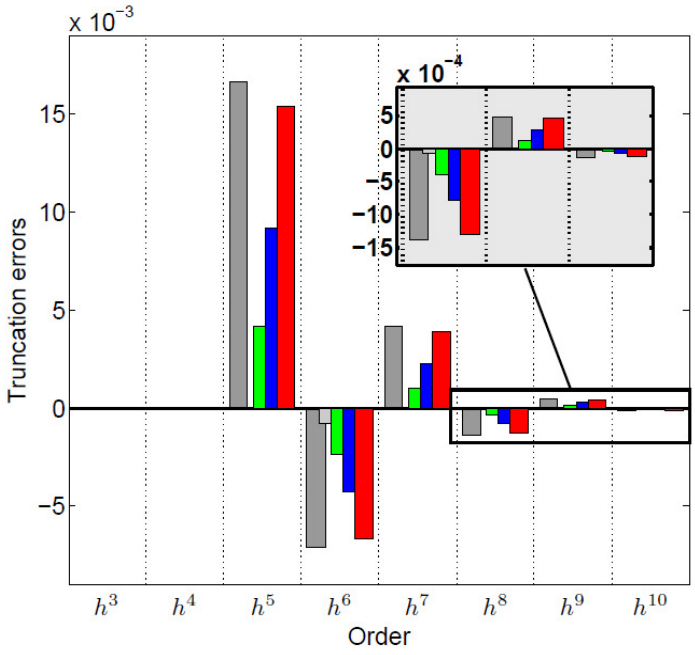

Figure 10. Truncation errors in smooth regions. WENO (dark grey), WCS (light grey), and MWCS ($\overline{\lambda} = 0.0$ green, $\overline{\lambda} = 0.4$ blue, $\overline{\lambda} = 0.9$ red).

Shock region: using only stencil E_0

In the case of a shock contained in the stencils E_1 and E_2, the values of the non-linear weights in Eq. (3.5) are substituted in Eq. (4.2), obtaining the truncation error of the WENO and WCS when only stencil E_0 is used for the approximation

$$\tau^{(WENO)} = \frac{1}{4}h^3\frac{\partial^4 F_j}{\partial x^4} - \frac{3}{10}h^4\frac{\partial^5 F_j}{\partial x^5} + \frac{5}{24}h^5\frac{\partial^6 F_j}{\partial x^6} - \frac{3}{28}h^6\frac{\partial^7 F_j}{\partial x^7} + \frac{43}{960}h^7\frac{\partial^8 F_j}{\partial x^8} - \frac{23}{1440}h^8\frac{\partial^9 F_j}{\partial x^9} + \frac{121}{24192}h^9\frac{\partial^{10} F_j}{\partial x^{10}} - \frac{311}{221760}h^{10}\frac{\partial^{11} F_j}{\partial x^{11}} + o\left(h^{12}\right) \tag{4.6a}$$

$$\tau^{(WCS)} = \frac{1}{12}h^3\frac{\partial^4 F}{\partial x^4} - \frac{1}{15}h^4\frac{\partial^5 F}{\partial x^5} + \frac{11}{360}h^5\frac{\partial^6 F}{\partial x^6} - \frac{13}{1260}h^6\frac{\partial^7 F}{\partial x^7} + \frac{19}{6720}h^7\frac{\partial^8 F}{\partial x^8} - \frac{1}{1512}h^8\frac{\partial^9 F}{\partial x^9} + \frac{257}{1814400}h^9\frac{\partial^{10} F}{\partial x^{10}} - \frac{19}{739200}h^{10}\frac{\partial^{11} F}{\partial x^{11}} + o\left(h^{12}\right) \tag{4.6b}$$

Figure 11 shows the truncation errors for the WENO, WCS and MWCS in form of a bar plot w.r.t. different considered orders, when only the stencil E_0 is used for the approximation. The following conclusions can be drawn:

- the MWCS has lower truncation errors w.r.t. WENO for all the considered orders;
- the magnitude of the errors for the WCS is considerably lower w.r.t. WENO for all orders considered;
- the leading term of the truncation error for the MWCS is $\sim 10^{-1}h^3$, and the magnitude of the errors decreases to $\sim 10^{-2}$ from the order h^6 and above.

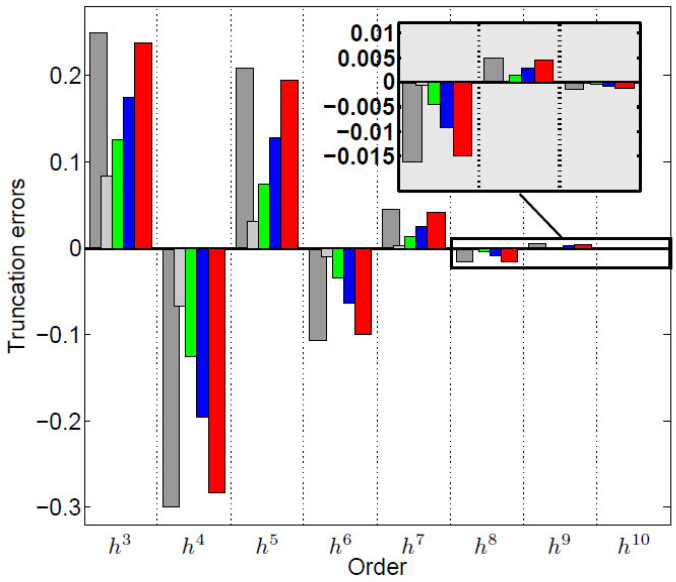

Figure 11. Truncation errors when only stencil E_0 is used. WENO (dark grey), WCS (light grey), and MWCS ($\bar{\lambda} = 0.0$ green, $\bar{\lambda} = 0.4$ blue, $\bar{\lambda} = 0.9$ red).

Shock region: using only stencil E_1

In the case where stencils E_0 and E_2 contain a shock, the values of the non-linear weights reported in Eq. (3.8) are substituted in Eq. (4.2), obtaining for the truncation errors of WENO and WCS the following expressions

$$\tau^{(WENO)} = -\frac{1}{12}h^3\frac{\partial^4 F_j}{\partial x^4} + \frac{1}{30}h^4\frac{\partial^5 F_j}{\partial x^5} - \frac{1}{72}h^5\frac{\partial^6 F_j}{\partial x^6} + \frac{1}{252}h^6\frac{\partial^7 F_j}{\partial x^7} - \frac{1}{960}h^7\frac{\partial^8 F_j}{\partial x^8} + \frac{1}{4320}h^8\frac{\partial^9 F_j}{\partial x^9} - \frac{17}{362880}h^9\frac{\partial^{10} F_j}{\partial x^{10}} + \frac{17}{1995840}h^{10}\frac{\partial^{11} F_j}{\partial x^{11}} + o\left(h^{12}\right) \tag{4.7a}$$

$$\tau^{(WCS)} = \frac{1}{120}h^4\frac{\partial^5 F}{\partial x^5} + \frac{1}{2520}h^6\frac{\partial^7 F}{\partial x^7} + \frac{1}{120960}h^8\frac{\partial^9 F}{\partial x^9} - \frac{1}{26611200}h^{10}\frac{\partial^{11} F}{\partial x^{11}} + o\left(h^{12}\right) \tag{4.7b}$$

In Eq. (4.7b) for the WCS the even derivative terms are absent confirming the Fourier analysis in Section II, where it is shown that the central stencil of WCS is free from dissipation errors. Figure 12 reports the truncation errors for the WENO, WCS and MWCS in the form of a bar plot for the different considered orders of magnitude, when only stencil E_1 is used for the interpolation. The following considerations can be made:

- the MWCS has lower truncation errors w.r.t. WENO for all the considered orders;
- the WCS is free from dissipation errors, and the dispersive errors are considerably lower w.r.t. WENO;
- the leading truncation error for the MWCS is $\sim 10^{-2}h^3$, and the magnitude of the errors decreases rapidly for higher orders.

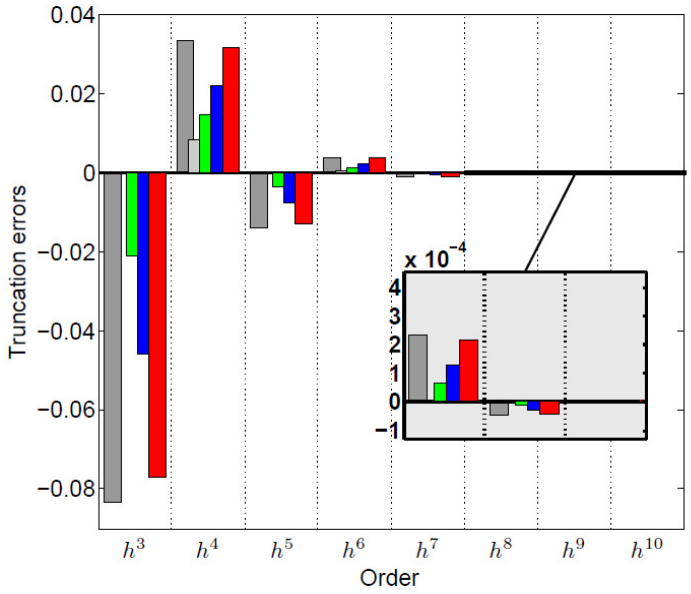

Figure 12. Truncation errors when only stencil E_1 is used. WENO (dark grey), WCS (light grey), and MWCS ($\bar{\lambda} = 0.0$ green, $\bar{\lambda} = 0.4$ blue, $\bar{\lambda} = 0.9$ red).

Shock region: using only stencil E_2

If the shock region is contained in stencils E_0 and E_1, the values of the non-linear weights as in Eq. (3.11) are substituted in Eq. (4.2) for obtaining the truncation errors of WENO and WCS when only stencil E_2 is used

$$\tau^{(WENO)} = \frac{1}{12}h^3\frac{\partial^4 F_j}{\partial x^4} + \frac{1}{30}h^4\frac{\partial^5 F_j}{\partial x^5} + \frac{1}{72}h^5\frac{\partial^6 F_j}{\partial x^6} + \frac{1}{252}h^6\frac{\partial^7 F_j}{\partial x^7} + \frac{1}{960}h^7\frac{\partial^8 F_j}{\partial x^8} + \frac{1}{4320}h^8\frac{\partial^9 F_j}{\partial x^9} + \frac{17}{362880}h^9\frac{\partial^{10} F_j}{\partial x^{10}} + \frac{17}{1995840}h^{10}\frac{\partial^{11} F_j}{\partial x^{11}} + o\left(h^{12}\right) \tag{4.8a}$$

$$\tau^{(WCS)} = -\frac{1}{12}h^3\frac{\partial^4 F}{\partial x^4} - \frac{1}{15}h^4\frac{\partial^5 F}{\partial x^5} - \frac{11}{360}h^5\frac{\partial^6 F}{\partial x^6} - \frac{13}{1260}h^6\frac{\partial^7 F}{\partial x^7} - \frac{19}{6720}h^7\frac{\partial^8 F}{\partial x^8} - \frac{1}{1512}h^8\frac{\partial^9 F}{\partial x^9} - \frac{257}{1814400}h^9\frac{\partial^{10} F}{\partial x^{10}} - \frac{19}{739200}h^{10}\frac{\partial^{11} F}{\partial x^{11}} + o\left(h^{12}\right) \tag{4.8b}$$

Figure 13 shows the bar plot of the truncation errors for WENO, WCS and MWCS for the considered orders, when only stencil E_2 is used for the interpolation. The following considerations can be drawn:

- the magnitude of the truncation error for the MWCS is lower w.r.t. both WENO and WCS for all considered orders;
- the truncation errors of WENO and WCS have comparable magnitudes, but opposite signs;
- the leading error term of MWCS is $\sim 10^{-2}h^3$, and the magnitude of the truncation errors decrease rapidly for higher orders.

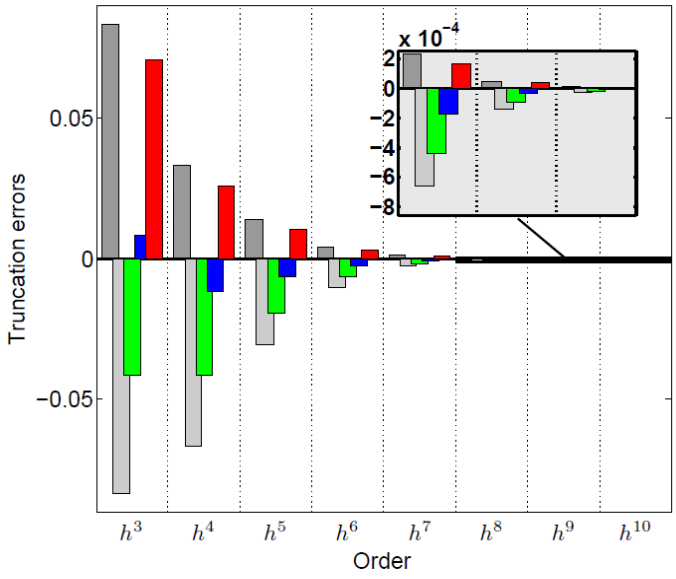

Figure 13. Truncation errors when only stencil E_2 is used. WENO (dark grey), WCS (light grey), and MWCS ($\bar{\lambda} = 0.0$ green, $\bar{\lambda} = 0.4$ blue, $\bar{\lambda} = 0.9$ red).

The local truncation error analysis confirms the considerations made in Section II and the results of the Fourier analysis presented in Section III, i.e. the proposed MWCS is 5th order accurate in smooth regions and the dissipation

and dispersion errors (respectively the even and odd derivative terms in the expressions for the truncation errors above) are lower compared to WENO and WCS in both smooth and shock regions. For shock regions, all considered schemes make use of a low-order accurate stencil, resulting in a leading error term $\sim 10^{-1}h^3$ for stencil E_0 and $\sim 10^{-2}h^3$ for stencils E_1 and E_2, nevertheless, the magnitude of the errors decreases for higher orders.

V. Numerical Results

The Euler equations for selected one- and two-dimensional test cases are solved by the proposed MWCS and compared against WENO[8] and WCS[30].

A. One-dimensional case

The one-dimensional Euler equations in vector and conservative form read as

$$\begin{gathered}\frac{\partial \mathbf{U}}{\partial t}+\frac{\partial \mathbf{F}}{\partial x}=0\\ \mathbf{U}=\left(\rho,\rho u,E_t\right)^T\\ \mathbf{F}=\left(\rho u,\rho u^2+p,u\left(E_t+p\right)\right)^T\end{gathered} \tag{5.1}$$

where $x\in(-5,5)$, and the grid is uniform with size $h=0.05$ (201 grid points). A Steger-Warming[38] flux-splitting is used, and the time quadrature is a third-order Runge-Kutta scheme.

Sod shock-tube problem

The shock-capturing capability of the MWCS is tested by the Sod shock-tube problem[39]. Equations (5.1) are solved coupled with the following initial conditions

$$\left(\rho,u,p\right)=\begin{cases}(1,0,1) & t=0,x\le 0\\ (0.125,0,0.1) & t=0,x>0\end{cases} \tag{5.2}$$

Figures 14-17 show the plot of the solved velocity u, at time $t=2$. Figures 14, 15 and 16 report the solution on the whole domain for MWCS, WCS and WENO schemes, respectively. The reference solution is regarded as the one obtained by the fifth-order WENO scheme using a mesh of 1600 points, labeled as WENO 1600. All the other simulations are carried out on a coarser mesh of 200 points. The solutions using MWCS (labeled as MWCS 200) and WENO scheme (labeled as WENO 200) are free from visible oscillations, which on the contrary, are present for WCS (labeled as WCS 200). Figure 17 reports an enlargement of the downstream shock area, comparing the three different schemes. Using MWCS scheme, the discontinuity is captured more sharply and is less smeared compared to the fifth-order WENO, and the solution does not present unphysical oscillations, which on the contrary affect the WCS solution.

Figure 18 reports the results for the shock-sensor proposed in (2.16) after the application of the Gaussian filtering (2.17), used for the solution of the shock-tube problem (5.1, 5.2) by MWCS. The location of the compression shock is properly detected by the sensor, while the upstream expansion wave does not activate the detection being associated with a positive value of the divergence of the velocity vector.

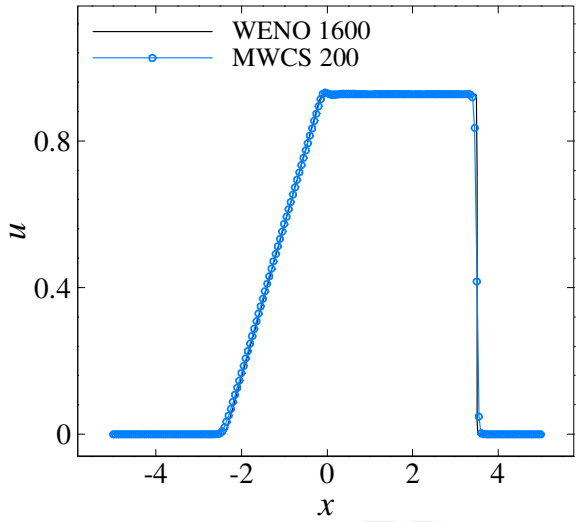

Figure 14. MWCS solution to problem (5.1) coupled with initial conditions (5.2).

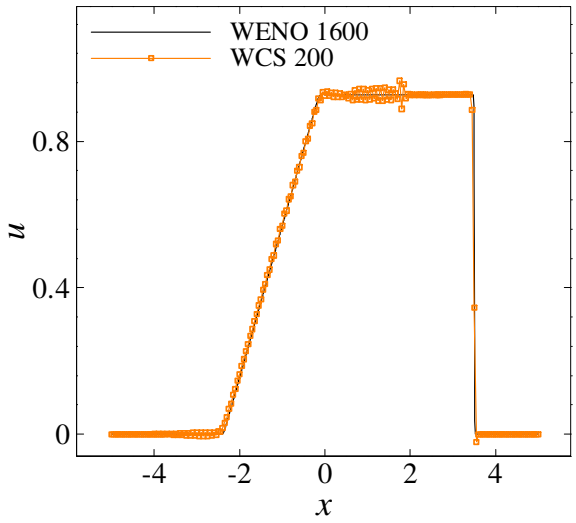

Figure 15. WCS solution to problem (5.1) coupled with initial conditions (5.2).

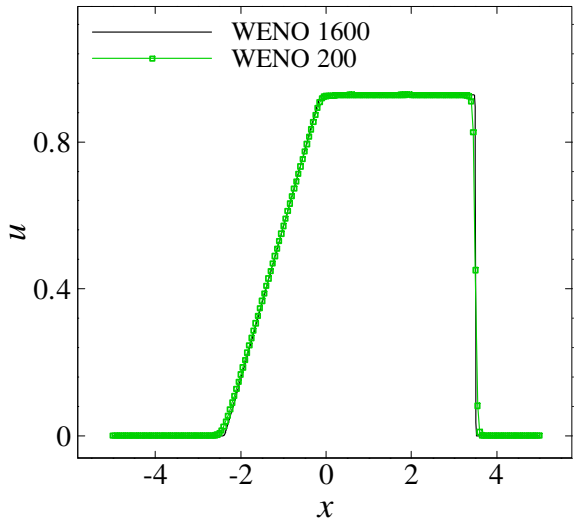

Figure 16. WENO solution to problem (5.1) coupled with initial conditions (5.2).

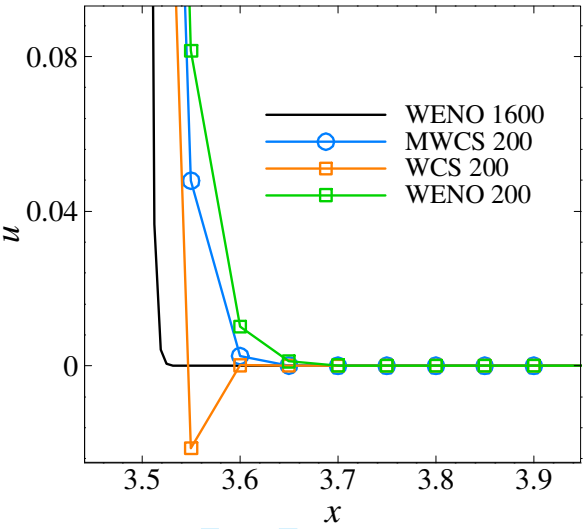

Figure 17. Enlargement of the MWCS,WCS and WENO solution to problem (5.1) coupled with initial conditions (5.2).

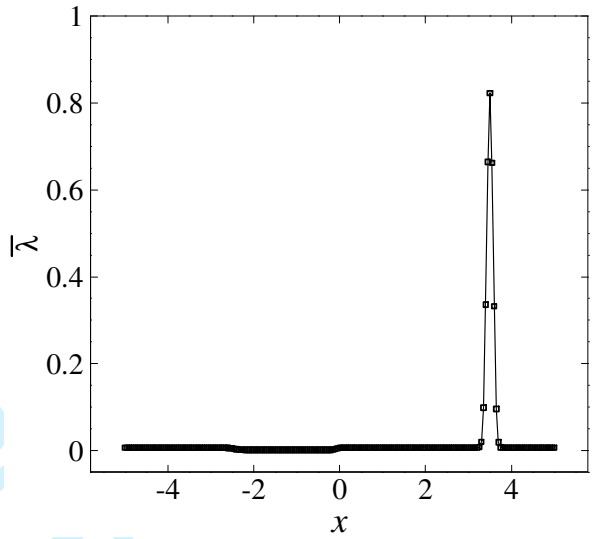

Figure 18. The shock-sensor proposed in (2.16, 2.17) for the shock-tube problem (5.1, 5.2).

Shu-Osher problem

The shock-entropy wave interaction problem[5] is solved in order to test the proposed method's capability on shock-capturing and shock-turbulence interaction. The entropy waves are very sensitive to numerical dissipation introduced by a numerical scheme, and can be excessively damped. Equations (5.1) are solved, coupled with the following initial condition

$$(\rho, u, p) = \begin{cases} (3.857143, 2.629369, 10.33333) & t = 0, x < -4 \\ (1 + 0.2\sin(5x), 0, 1) & t = 0, x \geq -4 \end{cases} \tag{5.3}$$

Figures 19-24 show the result for the solved density distribution ρ at time $t = 1.8$. Figures 19, 20 and 21 report the solution on the whole domain for MWCS, WCS and WENO schemes, respectively. The reference solution is regarded as the one obtained by the fifth-order WENO scheme using a mesh of 1600 points, labeled as WENO 1600. All the other calculations are made on a coarser mesh of 200 points. The MWCS scheme (labeled MWCS 200) shows higher resolution and sharper shock capturing compared to WENO (labeled WENO 200). WCS (labeled WCS 200) is capable of capturing the high-frequencies waves generated in the upstream area of the shock, due to the intrinsic non-dissipative nature of the scheme. Figures 22, 23 and 24 report detail enlargements of discontinuity areas in the upstream shock region, comparing the three different schemes. It can be observed that MWCS solution, compared to the fifth-order WENO solution, can capture the shock more sharply and has better resolution properties, and is free from numerical oscillations. In certain areas, the WCS appears to be very close to the reference solution, but is affected by numerical oscillations (see, for instance, Fig. 23).

Figure 25 reports the results for the shock-sensor proposed in (2.16) after the application of the Gaussian filtering (2.17), used to solve the shock-entropy problem (5.1, 5.3) by MWCS. The location of the main compression shock is properly detected, together with the location and magnitude of the minor upstream shocks.

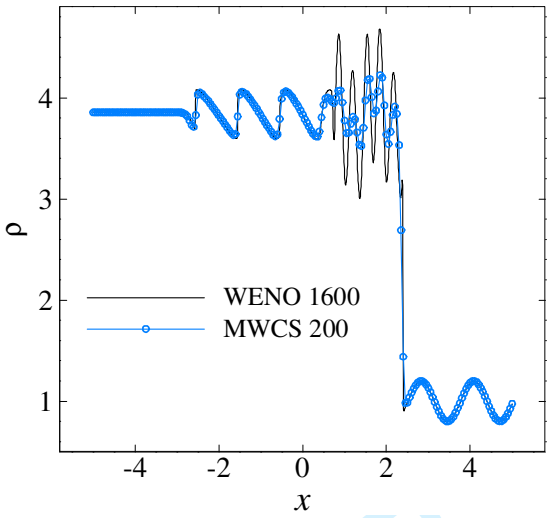

Figure 19. MWCS solution to problem (5.1) coupled with initial conditions (5.3).

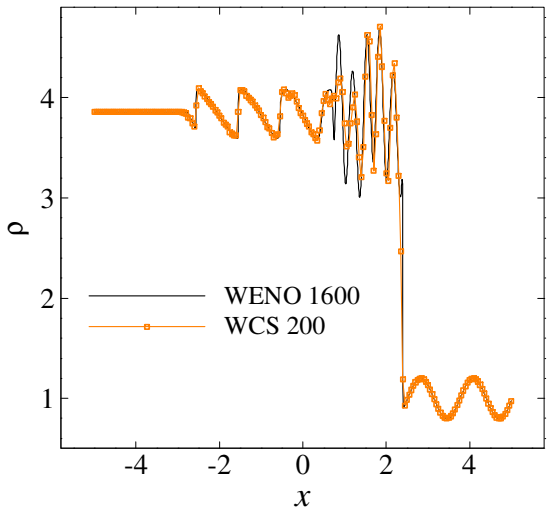

Figure 20. WCS solution to problem (5.1) coupled with initial conditions (5.3).

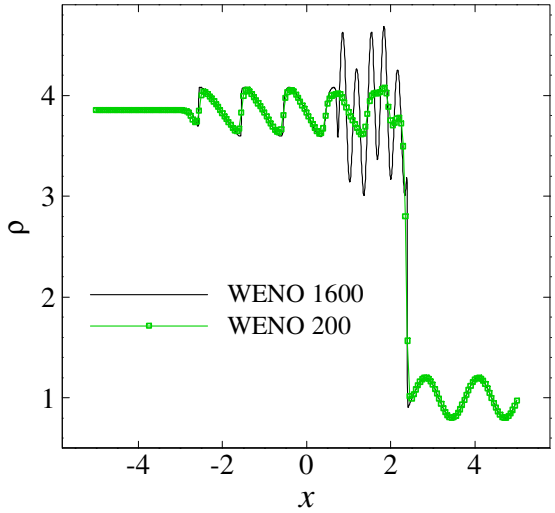

Figure 21.WENO solution to problem (5.1) coupled with initial conditions (5.3).

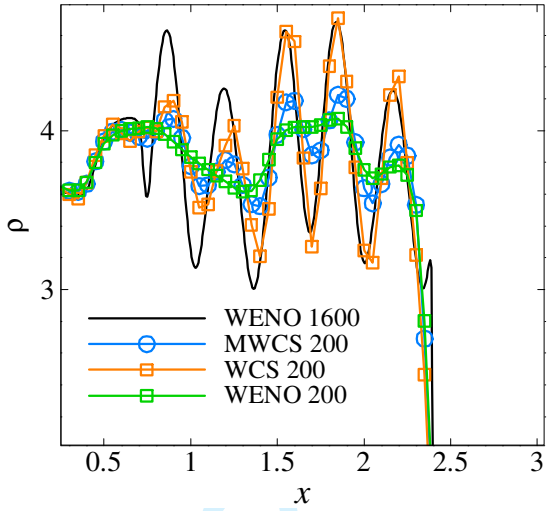

Figure 22. Enlargement of MWCS, WCS and WENO solution to problem (5.1) coupled with initial conditions (5.3).

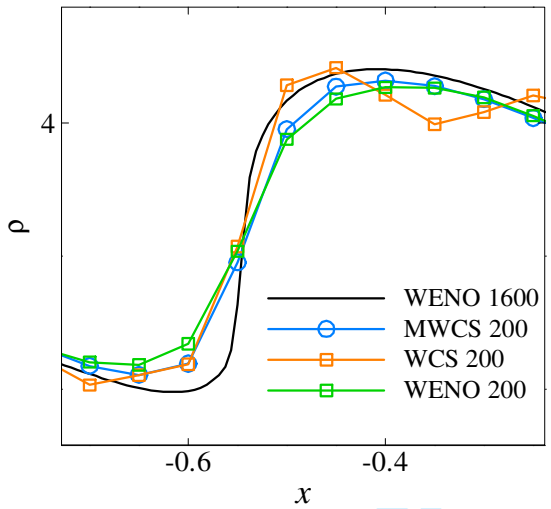

Figure 23. Enlargement of MWCS, WCS and WENO solution to problem (5.1) coupled with initial conditions (5.3).

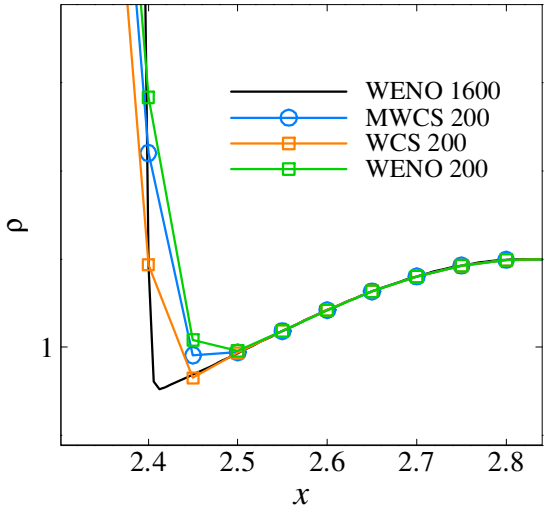

Figure 24. Enlargement of MWCS, WCS and WENO solution to problem (5.1) coupled with initial conditions (5.3).

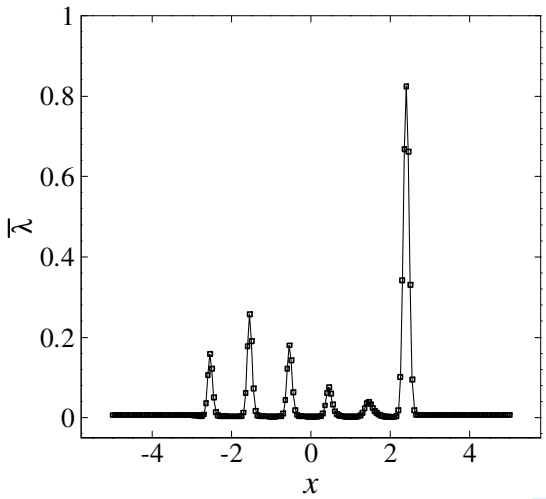

Figure 25. The shock-sensor proposed in (2.16, 2.17) for the shock-enropy problem (5.1, 5.3).

B. Two-dimensional case

The two-dimensional Euler equations in vector and conservative form read as

$$\begin{aligned} &\frac{\partial \mathbf{U}}{\partial t}+\frac{\partial \mathbf{F}}{\partial x}+\frac{\partial \mathbf{G}}{\partial y}=0 \\ &\mathbf{U}=\left(\rho,\rho u,\rho v,E_t\right)^T \\ &\mathbf{F}=\left(\rho u,\rho u^2+p,\rho uv,u\left(E_t+p\right)\right)^T \\ &\mathbf{G}=\left(\rho v,\rho uv,\rho v^2+p,v\left(E_t+p\right)\right)^T \end{aligned} \tag{5.4}$$

where $x\in(0,2)$, $y\in(0,1.1)$, and uniform grid of $65x65$ points is used. The Lax-Friedrichs flux-splitting is used, and the time quadrature is a third-order Runge-Kutta scheme. The test case is the oblique shock reflection on

an inviscid wall, with shock angle of 35.24° and the Mach 2 freestream. The shock jump conditions at the upper and the slip-wall conditions at the lower boundary are imposed, the inflow conditions are fixed to the freestream and the outflow conditions are calculated by extrapolation.

Figures 26-28 show the contour of the pressure p, for the analytical, MWCS and WENO solutions respectively (the WCS excessive numerical oscillations prevent from getting a solution in this test case). Comparing the two schemes, it is observed that the MWCS captures the shock more sharply than WENO scheme, and does not present important numerical oscillations.

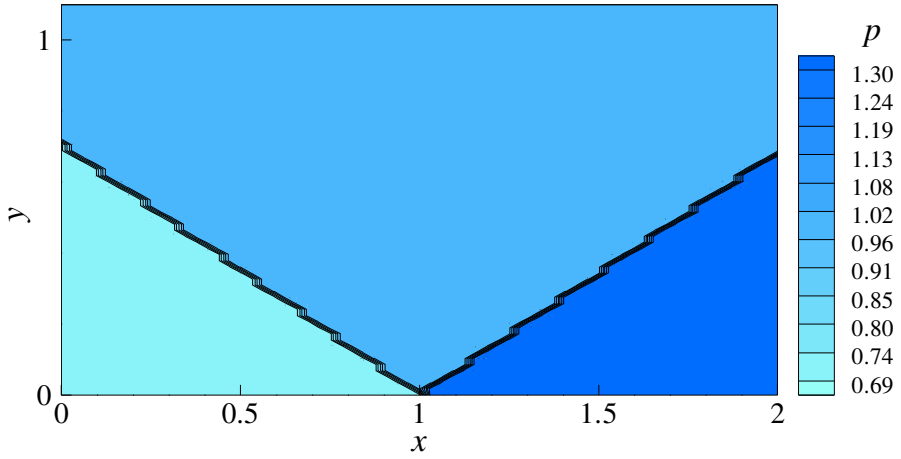

Figure 26. Analytic solution for the Mach 2 oblique shock reflection. Pressure, 12 equally spaced contours.

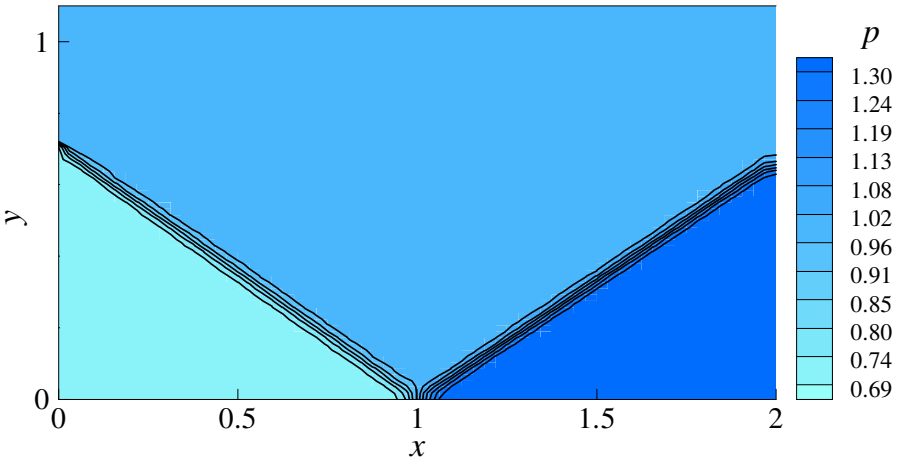

Figure 27. MWCS solution for the Mach 2 oblique shock reflection. Pressure, 12 equally spaced contours.

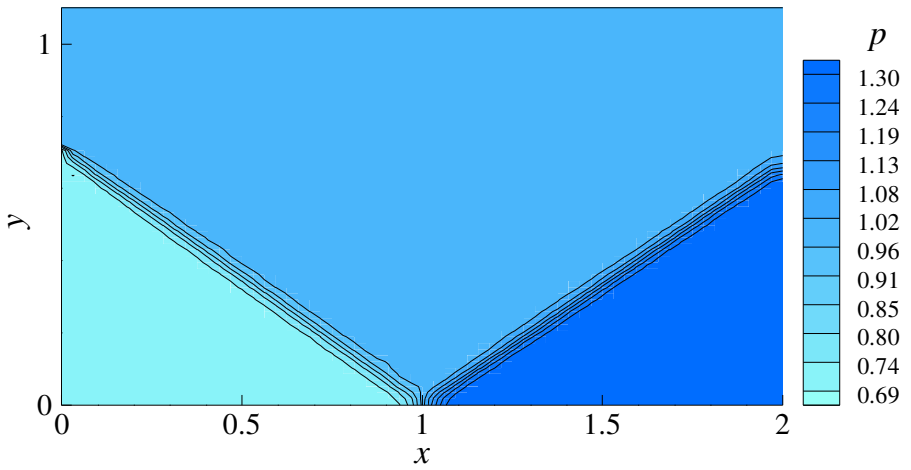

Figure 28. WENO solution for the Mach 2 oblique shock reflection. Pressure, 12 equally spaced contours.

Figures 29 and 30 report the pressure distribution for the Mach 2 oblique shock reflection for $y = 0$ and $y = 0.34$, respectively, for the analytical solution, MWCS and WENO. We can observe that the MWCS solution compared to WENO is capable of capturing the shock more sharply, without generating important numerical oscillations. Enlargements of shock regions for the pressure distribution at $y = 0.34$ are reported in Fig. 31 and Fig. 32, confirming that MWCS smears the shock less than WENO, without generating important numerical oscillations.

Figure 33 reports the results for the shock-sensor proposed in (2.16) after the application of the Gaussian filtering (2.17), used to solve the oblique shock reflection problem by MWCS. The location of the main compression shock is accurately detected in the whole domain.

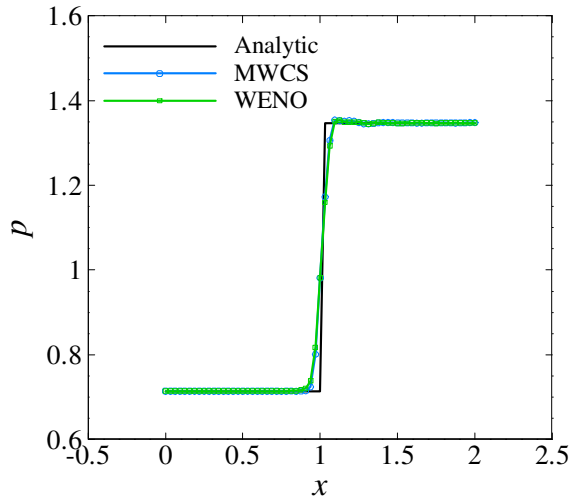

Figure 29. Analytic, MWCS and WENO solution for the Mach 2 oblique shock. Pressure distribution at $y = 0$.

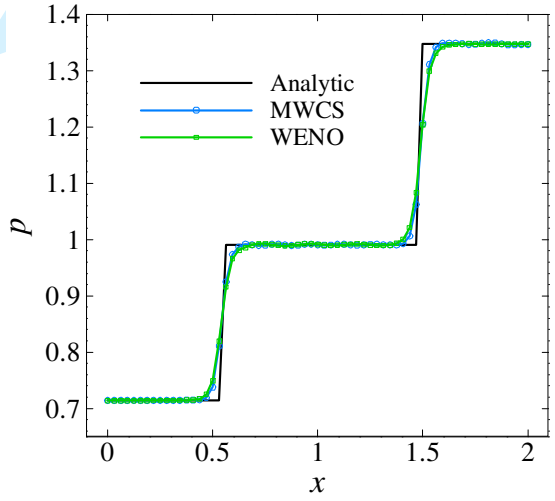

Figure 30. Analytic, MWCS and WENO solution for the Mach 2 oblique shock. Pressure distribution at $y = 0.34$.

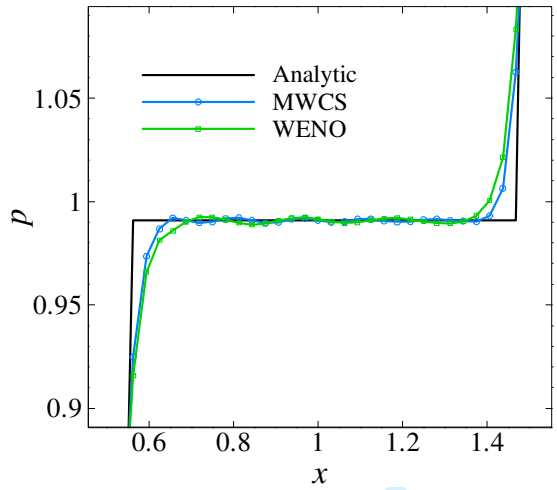

Figure 31. Analytic, MWCS and WENO solution for the Mach 2 oblique shock. Enlargement of pressure distribution at $y = 0.34$.

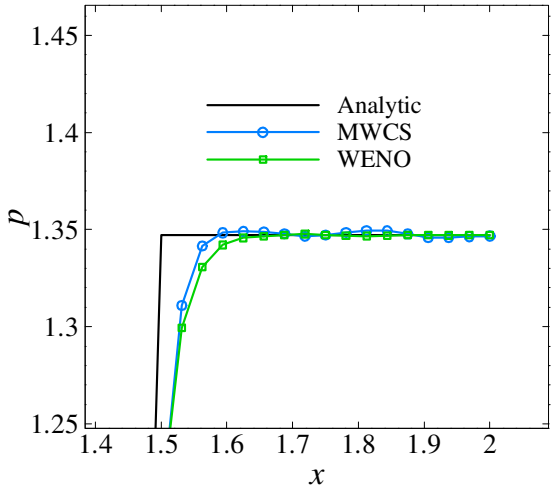

Figure 32. Analytic, MWCS and WENO solution for the Mach 2 oblique shock. Enlargement of pressure distribution at $y = 0.34$.

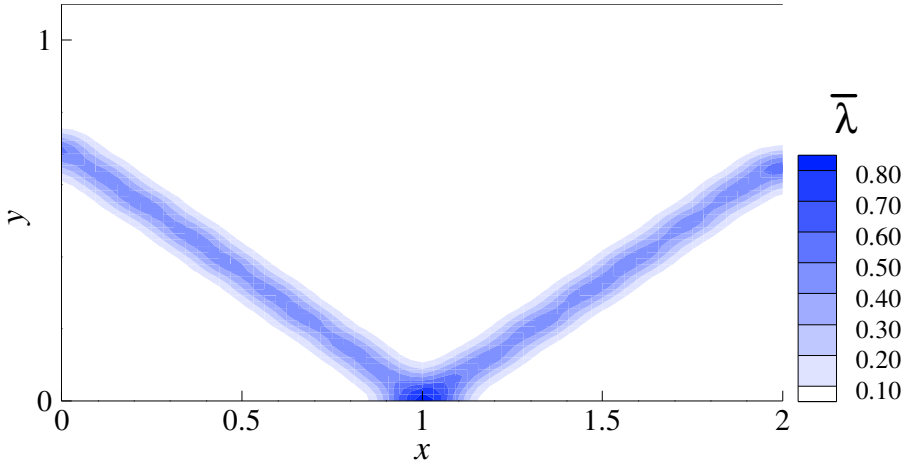

Figure 33. The shock-sensor proposed in (2.16, 2.17) for the oblique shock reflection problem.

C. Considerations on Computational Efficiency

The 1D Sod's shock-tube problem (solving equations (5.1) with initial conditions (5.2)) is chosen, and the CPU time consumption is measured using, one at a time, each of the three different subroutines for the WENO, WCS and MWCS for the solution of the problem. In other words, only the code efficiency of the three different subroutines for the high-order calculation of the derivative of a discrete input function is here assessed, while the rest of the code for the solution of the problem is kept unchanged, thus assuring a fair comparison of the three schemes. The computations are carried out on an Intel® Core™ 2 Duo CPU P9600, 2.53GHz machine. All the CPU times are in seconds, and the reported values are the average over five runs for each case. For the sake of reference, a scaling CPU time value is provided, and namely the benchmark proposed by Ref. 40 is solved for the double precision calculation of the product of two random sparse matrices of 1024×1024 elements, resulting in the consumption of $19.18\,sec$ of CPU time on the aforementioned machine. All numerical tests for the CPU efficiency are compiled with the "-r8 -O0" flag. Table 1 reports the CPU time consumed for each of the three schemes for different refinements of the mesh, and the relative ratios of the CPU time, obtained simply by averaging the ratios for the different meshes.

Table 1. CPU time consumption of the different schemes WENO, WCS and MWCS for the solution of the 1D Sod's shock-tube problem (5.1) with initial conditions (5.2). Relative ratios are reported for comparison.

	Number of mesh nodes			Comparison CPU time relative ratios		
Scheme:	201	401	801	WENO	WCS	MWCS
WENO	0.178 *sec*	0.678 *sec*	2.694 *sec*	1.00	0.66	0.41
WCS	0.266 *sec*	1.032 *sec*	4.130 *sec*	1.52	1.00	0.63
MWCS	0.424 *sec*	1.642 *sec*	6.622 *sec*	2.42	1.60	1.00

.

The following considerations can be made:

- as already mentioned in Section II when describing the different schemes, the WENO scheme does not involve the solution of any matrix for the computation of the high-order derivative, and consequently it turns out to be computationally more efficient among the three considered schemes; the calculation of the smoothness indicators (2.9) and the non-linear weights (2.8) constitutes apparently the most costly part of the WENO scheme;
- the WCS involves the solution of a tri-diagonal matrix of size $N+1$, which is calculated using the Thomas algorithm; furthermore, the WCS requires the calculation of the smoothness indicators (2.9), which are exactly the same as used in the WENO scheme, and are then used for calculating the non-linear weights (2.8), which on the contrary are different from WENO scheme since WCS uses a different set of optimal weights (2.12); the WCS thus results in a more computationally demanding scheme w.r.t. WENO;
- the MWCS, being a linear combination of the two schemes WENO and WCS, requires both the evaluation of the non-linear weights (2.8) (which differ for the two schemes, so the number of operations is doubled), and the solution of the tri-diagonal matrix after the linear combination of the schemes (2.15); the calculation of the smoothness indicators (2.9) is performed only once since it is exactly the same for both WENO and WCS; finally, the MWCS requires the use of the shock-detector (described in Section 2, Subsection D) for operating the linear blending between WENO and WCS, but its evaluation is of little influence on the CPU cost since it is evaluated only once at the beginning of each step of the time integration cycle (e.g., if using a three-step time Runge-Kutta scheme, the shock detector is evaluated only once before the first RK sub-step); the MWCS results in the most costly among the considered schemes, since it requires almost the sum of the operations involved in the WENO and WCS separately.

VI. Conclusion

The basic formulation of the MWCS, which is a linear combination of the WCS and WENO schemes without the introduction of any case-related adjustable parameter, is revised. A new formulation of the mixing function based on a shock-sensor is proposed and the Fourier analysis is used to assess the dispersion and dissipation errors in smooth and shock regions, showing that the proposed MWCS has higher resolution and lower dissipation compared to the well established WENO scheme, and has better stability characteristics compared to WCS. The local truncation error analysis shows that the magnitude of the truncation errors for the proposed MWCS are lower than WENO for both smooth and shock regions. The computational cost of MWCS is assessed in terms of CPU time consumption and compared to the pure WENO and WCS scheme, and, being MWCS a combination of these last two, it results in the most expensive scheme. Numerical tests carried out for inviscid flows problems in one- and two-dimensional cases confirm the results of the Fourier analysis, and demonstrate the proposed method's capability of capturing the shock sharply and without the generation of important numerical oscillations. The proposed shock-sensor formula detects accurately the compression shock location in all the considered numerical tests.

References

[1]Lele, S. K., "Compact finite difference schemes with spectral-like resolution", *Journal of Computational Physics,* Vol. 103, 1992, pp. 16–42.

[2]Visbal, M., & Gaitonde, D., "On the use of higher-order finite-difference schemes on curvilinear and deforming meshes", *Journal of Computational Physics,*Vol. 181, 2002, pp. 155–158.

[3]Yee, H. C., "Explicit and implicit multidimensional compact high-resolution shock-capturing methods: formulation", *Journal of Computational Physics*,Vol. 131, 1997, pp. 216–232.

[4]Shu, C. W., & Osher, S., "Efficient implementation of essentially non-oscillatory shock-capturing scheme", *Journal of Computational Physics*,Vol. 77, 1988, pp. 439–471.

[5]Shu, C. W., & Osher, S., "Efficient implementation of essentially non-oscillatory shock-capturing schemes II", *Journal of Computational Physics,* Vol. 83, 1989, pp. 32–78.

[6]Harten, A., Engquist, B., Osher, S., & Chakravarthy, S. R., "Uniformly high order accurate essentially non-oscillatory schemes, III", *Journal of Computational Physics,*Vol. 131, 1997, pp. 3–47.

[7]Liu, D., Osher, S., & Chan, T., "Weighted essentially non-oscillatory schemes", *Journal of Computational Physics*, Vol. 115, 1994, pp. 200–212.

[8]Jiang, G. S., & Shu, C. W., "Efficient implementation of weighted ENO scheme", *Journal of Computational Physics ,*Vol. 126, 1996, pp. 202–228.

[9]Shu, C. W., "High oder weighted essentially non-oscillatory schemes for convection dominated problems", *SIAM Review,*Vol. 51, 2009, pp. 82–126.

[10]Cockburn, B., Lin, S. Y., & Shu, C. W., "TVB Runge-Kutta local projection discontinuous Galerkin finite element method for conservation laws III: one-dimensional systems", *Journal of Computational Physics,*Vol. 84, 1989, pp. 90–113.

[11]Cockburn, B., & Shu, C. W., "The local discontinuous Galerkin method for time-dependent convection-diffusion systems", *SIAM Journal on Numerical Analysis* , Vol. 35, 1998, pp. 2440–2463.

[12]Cockburn, B., "Discontinuous Galerkin methods", *Journal of Applied Mathematics and Mechanics*, Vol. 11, 2003, pp. 731–754.

[13]Bassi, F., & Rebay, S., "A high-order accurate discontinuous finite element menthod for the numerical solution of the compressible Navier-Stokes equations", *Journal of Computational Physics*, Vol. 131, 1997, pp. 267–279.

[14]Patera, A., "A spectral element method for fluid dynamics: Laminar flow in a channel expansion", *Journal of Computational Physics*, Vol. 54, 1984, pp. 468–488.

[15]Wang, Z., & Huang, G. P., "An essentially non-oscillatory high-order Padé-type (ENO-Padé) scheme", *Journal of Computational Physics*, Vol. 177, 2002, pp. 37–58.

[16]Liu, Y., Vinokur, M., & Wang, Z. J., "Spectral (finite) volume method for conservation laws on unstructured grids. V: extension to three-dimensional systems", *Journal of Computational Physics*, Vol. 212, 2006, pp. 454–472.

[17]Liu, Y., Vinokur, M., & Wang, Z. J., "Spectral difference method for unstructured grids I: basic formulation", *Journal of Computational Physics,* Vol. 216, 2006, pp. 780–801.

[18]Sun, Y., Wang, Z. J., & Liu, Y., "High-order multi-domain spectral difference method for the Navier-Stokes equations on unstructured hexahedral grids", *Communications in Computational Physics*,Vol. 2, 2007, pp. 310–333.

[19]Yee, H. C., Sjogreen, B., Sandham, N. D., & Hadjadj, A., "*Progress in the development of a class of efficient low dissipative high order shock-capturing methods",* Proceeding of the Symposium in Computational Fluid Dynamics for the 21st Century, 2000, Kyoto.

[20]Ma, Y., & Fu, D., "Forth order accurate compact scheme with group velocity control (GVC)", *Science in China,* Vol. 44, 2001, pp. 1197–1204.

[21]Adams, N. A., & Shariff, K. A high-resolution hybrid compact-ENO scheme for shock-turbulence interaction problems. *Journal of Computational Physics*, Vol. 127, 1996, pp. 27–51.

[22]Wang, Z. J., "Spectral (finite) volume method for conservation laws on unstructured grids: basic formulation", *Journal of Computational Physics*, Vol. 178, 2002, pp. 210–251.

[23]Godunov, S. K., "A difference method for numerical calculation of discontinuous solutions of the equations of hydrodynamics", *Mat. Sb. (N.S.)*, Vol. 47, No. 89, 1959, pp. 271–306.

[24]Roe, P. L., "Approximate Riemann solvers, parameter vectors, and difference schemes", *Journal of Computational Physics,* Vol. 43, No. 2, 1981, pp. 357–372.

[25]van Leer, B., "Towards the ultimate conservative difference scheme V. A second-order sequel to Godunov's method", *Journal of Computational Physics*, Vol. 135, 1997, pp. 229–248.

[26]Harten, A., "High resolution schemes for hyperbolic conservation laws", *Journal of Computational Physics,*Vol. 49, 1983, pp. 357–393.

[27]Kim, D., & Kwon, J., "A high-order accurate hybrid scheme using a central flux scheme and a WENO scheme for compressible flowfield analysis", *Journal of Computational Physics*, Vol. 210, 2005, pp. 554–583.

[28]Costa, B., & Don, W. S., "High order hybrid central-WENO finite difference scheme for conservation laws", *Journal of Computational and Applied Mathematics*, Vol. 204, 2007, pp. 209–218.

[29]Ren, Y., Liu, M., & Zhang, H., "A characteristic-wise hybrid compact-WENO scheme for solving hyperbolic conservation laws", *Journal of Computational Physics*, Vol. 192, 2003, pp. 365–386.

[30]Jiang, L., Shan, H., & Liu, C., "Weighted compact scheme for shock capturing", *International Journal of Computational Fluid Dynamics*, Vol. 15, 2001, pp. 147–155.

[31]Shu, C. W., "Essentially non-oscillatory and weighted essentially non-oscillatory schemes for hyperbolic conservation laws", NASA techical report 870251, 1997.

[32]Oliveira, M. L., "*High-order numerical schemes for high-speed flows",* PhD dissertation, Mathematics dept., University of Texas at Arlington, Arlington, TX, 2009.

[33]Harten, A., "The artificial compression method for computation of shocks and contact discontinuities: III. Self-adjusting hybrid schemes", *Mathematics of Computation,* Vol. 32, No. 142, 1978, pp. 363–389.

[34]Bhagatwala, A., Lele, S.K, "A modified artificial viscosity approach for compressible turbulence simulations", *Journal of Computational Physics*, Vol. 228, No. 14, 2009, pp. 4965–4969.

[35] Cook, A. W., & Cabot, W. H., "A high-wave number viscosity for high-resolution numerical methods", *Journal of Computational Physics*,Vol. 195, No. 2, 2004, 594–601.

[36] Vichevenetsky, R. V., & Bowles, J. B., *Fourier analysis of numerical approximations of hyperbolic equations.* Philadelphia: SIAM, 1982.

[37]Anderson, J. D., *Computational fluid dynamics.* New York: Mc Graw Hill, 1995.

[38]Steger, J., & Warming, R., "Flux vector splitting of the inviscid gasdynamic equations with applications to finite-difference methods", *Journal of Computational Physics,*Vol. 40, 1981, pp. 263–293.

[39]Sod, G. A., "A survey of several finite difference methods for systems on non-linear hyperbolic conservation laws", *Journal of Computational Physics,* Vol. 27, No. 1, 1978, pp. 1–31.

[40]W. F. Eddy, "The DECstation 3100 – UNIX for power users", *Chance*, Vol. 3, No. 2, 1990, pp.42–47.

Response to Referees

Manuscript ID GCOM-2012-0484-B, entitled "High-Order Weighted Compact and Non-Compact Scheme for Shock and Small Lenght Scale Interaction", by G. Stipcich, H. Fu, C. Liu.

General remarks:

In the following, Referee's remarks are numbered as Q1, Q2,… and the corresponding replies are numbered as R1, R2,…

In the revised manuscript, the added/modified parts are highlighted by the use of a BLUE colored text.

Referee 1:

Q1. *In eq.(2.8), the smoothness indicator IS is mentioned, it is better to include its expression and make the elaboration more clear. Otherwise readers will guess is it the same as the eq(2.15) in section II.D.*

R1. A paragraph has been added below Equation (2.8), in which the role and the construction of the smoothness indicators are outlined; moreover, the explicit expressions for the smoothness indicators IS have been added (see Equations (2.9a, b, c) of the revised manuscript).

Q2. *In eq(2.8), the value of p is simply set as 2 and in section II.B line 2.8 it is chosen to be 1. A reason should be provided.*

R2. In both sections II.A and II.B an explanation has been added to motivate the choice of p=2 for WENO scheme and p=1 for WCS (see, respectively, the parts highlighted in blue color below equations (2.8) and (2.13) of the revised manuscript). For the WENO scheme, a clearer reference to Ref. 8 (Jiang, G. S., & Shu, C. W., "Efficient implementation of weighted ENO scheme", *Journal of Computational Physics* ,Vol. 126, 1996, pp. 202–228) is made, where from numerical experiments the parameter is set p=2, finding it adequate to obtain essentially non-oscillatory approximations in applications with shocks. Analogously, for the WCS it is explicitly stated that from numerical experiments carried out by the authors, the parameter is set p=1 since it is observed to be adequate for the stability and shock-capturing property of the scheme.

Q3. *The coefficients in eq.(2.11) are titled "optimal". How the optimization was carried out?*

R3. A small paragraph has been added before Equation (2.11) of the original manuscript, which is Equation (2.12) of the revised manuscript, where the "optimal" weights for the WCS scheme are introduced. An explication is there provided for the aforementioned constant weights to be called "optimal". The constant values are chosen so as to recover, in smooth regions, the standard sixth-order accuracy compact scheme of Lele, S. K., "Compact finite difference schemes with spectral-like resolution," *Journal of Computational Physics,* Vol. 103, 1992, pp. 16-42, being the sixth-order the highest order of accuracy attainable from the weighted (convex) combination of the three lower order approximations coming from the three stencils ((2.10a,b,c) of the original manuscript, (2.11a,b,c) of the revised manuscript). Furthermore, after Equation (2.12) of the original manuscript (Equation (2.13) of the revised manuscript) the sentence has been changed, as highlighted in blue color, as to make the aforementioned concept explicit and clear.

Referee 2:

Q1. *The proposed scheme seems to be less dissipative than the pure WENO, indicating 'better' performance in this respect. However, at the same time, the authors may want to comment on the computational cost/time of the proposed hybrid scheme, vs. the WENO. I suspect that the scheme is more expensive. But how much more expensive? Specifically, how is the computational cost of pure WCS compared with pure WENO scheme, and the proposed mixed scheme compared with the pure WENO? The authors may want to add some discussion about this, and in numerical section have some results (table of computational time for different schemes) reflect such discussion. Note that some discussion is needed besides a table of computational time, as code efficiency (how good a code is written) might play some role here.*

R1. A whole Subsection (Subsection C, in Section V) named "Considerations on Computational Efficiency" has been added. A specific one-dimensional problem is solved by the use, one at a time, of the three different schemes, i.e. WENO, WCS and MWCS. The CPU times are reported in Table 1, both in seconds and in terms of relative ratio, as to highlight the comparison among the three schemes, with a brief discussion on the implementation issues and features of each of the three schemes. It is explicitly stated that in order to have a fair comparison between the three schemes, the same "main" code is used, but for each of three schemes simply the associated subroutine is used for the calculation of the derivative of the discrete variables involved in the problem. The technical specification of the machine used for the calculations is reported, along with the CPU time required for the solution of a benchmark problem, in order to provide a scaling factor for the CPU times in Table 1. A sentence has been added in the introduction Section I and in the conclusion Section VI (highlighted in blue), regarding the considerations on the computational efficiency of the scheme, and reference Ref. 40 has been added for the benchmark problem.